



HAL
open science

Estimating leaf mass per area and equivalent water thickness based on leaf optical properties: potential and limitations of physical modeling and machine learning.

Jean-Baptiste Féret, G. Le Maire, S. Jay, D. Berveiller, Ryad Bendoula, G. Hmimina, Anice Cheraiet, J.C. Oliveira, F.J. J Ponzoni, T. Solanki, et al.

► **To cite this version:**

Jean-Baptiste Féret, G. Le Maire, S. Jay, D. Berveiller, Ryad Bendoula, et al.. Estimating leaf mass per area and equivalent water thickness based on leaf optical properties: potential and limitations of physical modeling and machine learning.. Remote Sensing of Environment, 2019, 231, pp.110959. 10.1016/j.rse.2018.11.002 . hal-02939160

HAL Id: hal-02939160

<https://hal.inrae.fr/hal-02939160>

Submitted on 15 Sep 2020

HAL is a multi-disciplinary open access archive for the deposit and dissemination of scientific research documents, whether they are published or not. The documents may come from teaching and research institutions in France or abroad, or from public or private research centers.

L'archive ouverte pluridisciplinaire **HAL**, est destinée au dépôt et à la diffusion de documents scientifiques de niveau recherche, publiés ou non, émanant des établissements d'enseignement et de recherche français ou étrangers, des laboratoires publics ou privés.

1 Estimating leaf mass per area and equivalent water thickness based on leaf optical properties:
2 potential and limitations of physical modeling and machine learning.

3 J.-B. Féret¹, G. le Maire^{2,3,4}, S. Jay⁵, D. Berveiller⁶, R. Bendoula⁷, G. Hmimina⁶, A. Cheraiet⁶, J.C.
4 Oliveira⁸, F.J. Ponzoni⁹, T. Solanki¹⁰, F. de Boissieu¹, J. Chave¹¹, Y. Nouvellon^{2,3,12}, A. Porcar-Castell¹⁰, C.
5 Proisy^{13,14}, K. Soudani⁶, J.-P. Gastellu-Etchegorry¹⁵, M.-J. Lefèvre-Fonollosa¹⁶

6 ¹TETIS, Irstea, AgroParisTech, CIRAD, CNRS, Université Montpellier, Montpellier, France

7 ²CIRAD, UMR ECO&SOLS, Montpellier, France

8 ³Eco&Sols, Univ Montpellier, CIRAD, INRA, IRD, Montpellier SupAgro, Montpellier, France.

9 ⁴Interdisciplinary Center of Energy Planning (NIPE), UNICAMP, 13083-896 Campinas, Brazil

10 ⁵Aix Marseille Univ, CNRS, Centrale Marseille, Institut Fresnel, F-13013 Marseille, France

11 ⁶Ecologie Systematique Evolution, University of Paris-Sud, CNRS, AgroParisTech, Université Paris
12 Saclay, F-91400 Orsay, France

13 ⁷ITAP, Irstea, Montpellier SupAgro, Université Montpellier, Montpellier, France

14 ⁸School of Agricultural Engineering - FEAGRI, University of Campinas, São Paulo, Brazil

15 ⁹Instituto Nacional de Pesquisas Espaciais, Sao Jose dos Campos 12227-010, Brazil

16 ¹⁰Optics of Photosynthesis Laboratory, INAR/Forests, Faculty of Agriculture and Forestry, 00014
17 University of Helsinki, Finland

18 ¹¹Laboratoire Evolution et Diversité Biologique UMR 5174, CNRS, Université Paul Sabatier, Toulouse,
19 France

20 ¹²University of Sao Paulo, ESALQ/USP, Piracicaba 13418-900, Brazil

21 ¹³AMAP, IRD, CIRAD, CNRS, INRA, Univ. Montpellier, Montpellier, France

22 ¹⁴GEOSMIT, French Institute of Pondicherry, Pondicherry, India

23 ¹⁵Centre d'Etudes Spatiales de la Biosphère, Toulouse 31400, France

24 ¹⁶CNES

25 **Abstract**

26 Leaf mass per area (*LMA*) and leaf equivalent water thickness (*EWT*) are key leaf functional traits
27 providing information for many applications including ecosystem functioning modeling and fire risk
28 management. In this paper, we investigate two common conclusions generally made for *LMA* and
29 *EWT* estimation based on leaf optical properties in the near-infrared (NIR) and shortwave infrared
30 (SWIR) domains: (1) physically-based approaches estimate *EWT* accurately and *LMA* poorly, while
31 (2) statistically-based and machine learning (ML) methods provide accurate estimates of both *LMA*
32 and *EWT*.

33 Using six experimental datasets including broadleaf species samples of more than 150 species
34 collected over tropical, temperate and boreal ecosystems, we compared the performances of a
35 physically-based method (PROSPECT model inversion) and a ML algorithm (support vector machine
36 regressions, SVM) to infer *EWT* and *LMA* based on leaf reflectance and transmittance. We assessed
37 several merit functions to invert PROSPECT based on iterative optimization and investigated the
38 spectral domain to be used for optimal estimation of *LMA* and *EWT*. We also tested several
39 strategies to select the training samples used by the SVM, in order to investigate the generalization
40 ability of the derived regression models.

41 We evidenced that using spectral information from 1700 to 2400 nm leads to strong improvement in
42 the estimation of *EWT* and *LMA* when performing a PROSPECT inversion, decreasing the *LMA* and
43 *EWT* estimation errors by 55% and 33%, respectively.

44 The comparison of various sampling strategies for the training set used with SVM suggests that
45 regression models show limited generalization ability, particularly when the regression model is
46 applied on data fully independent from the training set. Finally, our results demonstrate that, when
47 using an appropriate spectral domain, the PROSPECT inversion outperforms SVM trained with
48 experimental data for the estimation of *EWT* and *LMA*. Thus we recommend that estimation of

49 *LMA* and *EWT* based on leaf optical properties should be physically-based using inversion of
50 reflectance and transmittance measurements on the 1700 to 2400 nm spectral range.

51

52 1. INTRODUCTION

53 Global climate change and biodiversity loss strongly impact species and ecosystem functions, which
54 directly influences processes at landscape and regional scales, and disrupts global biogeochemical
55 cycles (Chapin, 2003). These ecosystem functions are tightly connected with species composition
56 and can be partly described and explained using plant traits (Diaz and Cabido, 2001; Eviner and
57 Chapin, 2003). By definition, plant traits correspond to morphological, physiological or phenological
58 features measurable at the individual level, and functional traits are defined as these features
59 impacting individual fitness via their effects on growth, reproduction and/or survival, the three
60 components of individual performance (Violle et al., 2007). Therefore, our understanding of the
61 interactions between climate, human activity and ecosystem functioning strongly depends on our
62 capacity to monitor critical functional traits across space and time (Asner and Martin, 2016).

63 Leaf mass per area (*LMA*) is defined as the ratio of leaf dry mass (*DW*) to leaf area (*A*):

64

$$LMA = \frac{DW}{A} \text{ (mg.cm}^{-2}\text{)} \quad \text{Eq. 1}$$

65

66 It is a plant functional trait widely used as an indicator of plant functioning and ecosystem processes.

67 In the leaf economic spectrum theory, the biophysical constraints explain the high coordination
68 between organs properties and available resources: for instance, plants that have high trunk water
69 conductivity generally have high stomatal conductance, low *LMA* and high photosynthetic
70 capacities, developed root system and nutrient uptake, high turnover rate of resource acquisition
71 organs, high growth rates. *LMA* is therefore a very significant trait because it correlates with key

72 plant functional properties (de la Riva et al., 2016; Oren et al., 1986; Reich et al., 1997), therefore
73 capturing a great proportion of the functional variation in the ecosystem.

74 *LMA* is important for the description of plant strategies and photosynthetic capacity over various
75 vegetation types and climates (Asner et al., 2011; Gratani and Varone, 2006; Osnas et al., 2013;
76 Puglielli et al., 2015; Reich et al., 1997, 1998; Weng et al., 2017). It is also a predictor of relative
77 growth rate (Antúnez et al., 2001; Rees et al., 2010) and is usually correlated with mass-based
78 maximum photosynthetic rate (Wright et al. 2004). At broader scales, it is also identified as a critical
79 plant trait for the global monitoring of functional diversity, and for the determination of species
80 fitness in their environment, affecting various ecosystem processes (Poorter et al., 2009; Schimel et
81 al., 2015). Measurement of *LMA* is also relevant for many other applications, such as fire risk
82 assessment (Cornelissen et al., 2017). Finally, *LMA* allows the conversion of traits expressed on an
83 area basis into mass basis and vice versa. This is important since physical models usually express leaf
84 constituent content per surface unit, whereas ecologists and plant physiologists may use constituent
85 content per surface unit or per mass unit (Osnas et al., 2013; Wright et al., 2004).

86 The second important functional trait discussed in this study is the equivalent water thickness
87 (*EWT*), defined as:

88

$$EWT = \frac{FW - DW}{A} \text{ (mg.cm}^{-2}\text{)} \quad \text{Eq. 2}$$

89

90 with *FW* the leaf fresh mass. *EWT* is the area-weighted moisture content. It is related to a range of
91 physiological and ecosystem processes, including leaf-level tolerance to dehydration, and ecological
92 strategy. Indeed, species with large *EWT* tend to have lower construction costs, and are
93 predominantly fast-growing and pioneer species (Wright et al., 2004).

94 The ability to accurately estimate both *EWT* and *LMA* is also critical for applications such as fire
95 danger assessment: fuel moisture content (*FMC*, Chuvieco et al., 2002), also referred to as
96 gravimetric water content (*GWC*, Datt, 1999), is a critical variable affecting fire interactions with fuel
97 (Yebra et al., 2013). The accurate estimation of *FMC* is usually limited by the uncertainty associated
98 to the estimation of *LMA* (Riano et al., 2005). Destructive measurements of *LMA* and *EWT* are
99 time-consuming and logistically complex in remote environments. Alternative methods based on leaf
100 spectroscopy have showed good performances for the estimation of various constituents (Asner et
101 al., 2011, 2009; Ceccato et al., 2001; Colombo et al., 2008; Feilhauer et al., 2015; Féret et al., 2017;
102 Fourty and Baret, 1998). Two main types of methods have been developed for the estimation of
103 vegetation properties from their optical properties (including leaf chemistry but also canopy
104 biophysical properties): *physically-based* methods and *data-driven* methods, also referred to as
105 “radiometric data-driven approaches” and “biophysical variable driven approaches” respectively, by
106 Baret and Buis (2008). In this study, we will only use the terms physically-based methods and data-
107 driven methods in order to avoid confusion.

108 *Physically-based methods* are based on radiative transfer models (RTM) providing a mechanistic link
109 between leaf traits and their optical properties. They aim at minimizing the residuals between
110 measured and modeled radiometric data (hence the term “radiometric data-driven approach” by
111 Baret and Buis, 2008). The PROSPECT model (Jacquemoud and Baret, 1990; Féret et al., 2017) is the
112 most widespread model, due to its relative simplicity and computational efficiency combined with
113 excellent modeling performances for a broad range of leaf types. Several retrieval algorithms have
114 been developed to estimate leaf chemistry from their optical properties, taking advantage of
115 physical modeling. These include look-up-table (LUT) methods (Ali et al., 2016) and iterative
116 optimization based on minimization algorithms (Jacquemoud et al., 1996). Physically-based methods
117 do not require calibration data, but they are computationally demanding.

118 *Data-driven methods* use a calibration dataset of measured leaf optical properties and traits in order
119 to adjust regression models for the estimation of leaf chemistry (Verrelst et al., 2016). These include
120 regression models derived from spectral indices, one of the most classic approaches (Gitelson et al.,
121 2006; Main et al., 2011). More complex multivariate methods such as partial least square regression
122 (Asner et al., 2011), and machine learning algorithms (ML) are also extensively used in the domain of
123 remote sensing. These include support vector machine (SVM, Cortes and Vapnik, 1995; Drucker et
124 al., 1996), random forest (Breiman, 2001), and artificial neural networks (Hornik et al., 1989). ML
125 algorithms have been extensively used for remote sensing applications during the past decades,
126 most of them at the canopy level when it comes to the estimation of biochemical constituents
127 (Brown et al., 2000; Gualtieri, 2009; Lardeux et al., 2009; le Maire et al., 2011; Schmitter et al., 2017;
128 Stumpf and Kerle, 2011; Zhang et al., 2017) , and a limited number of studies focusing on the
129 leaf/needle scale (Conejo et al., 2015; Dawson et al., 1998; le Maire et al., 2004). ML algorithms
130 usually show good performances in terms of prediction ability and high computational efficiency.
131 The capacity of data-driven approaches to accurately predict leaf chemistry from their optical
132 properties is inherently dependent on the dataset used to train the algorithm and regression model.
133 The experiments performed in this study aim at quantifying this assertion over an extensive
134 experimental dataset. This implies that correct implementation of data-driven methods using
135 experimental data for training requires substantial efforts for the measurement of leaf optical
136 properties and chemical constituents with destructive methods, whereas physical modeling only
137 requires leaf optical properties.

138 Note that a third type of approach, namely, *hybrid* methods, could also be mentioned here (Verrelst
139 et al., 2015). Such methods use data-driven algorithms trained with spectral properties simulated
140 with physical models. These methods are particularly developed at the canopy scale, and combine

141 the advantages of physically-based and data-driven methods: they do not require destructive
142 measurements to build an experimental training dataset, and they are computationally efficient.

143 *LMA* and *EWT* both influence leaf optical properties in the near-infrared (NIR) and shortwave
144 infrared (SWIR) domains (Bowyer and Danson, 2004). However, physically-based methods have
145 often been reported to perform poorly for the estimation of *LMA* (Colombo et al., 2008; le Maire et
146 al., 2008; Riano et al., 2005; Wang et al., 2011). Several reasons have been mentioned in the
147 literature, including suboptimal modeling (Qiu et al., 2018), optical data collection (Merzlyak et al.,
148 2004) or inversion (Colombo et al., 2008; Qiu et al., 2018; Riano et al., 2005; Sun et al., 2018; Wang
149 et al., 2011, 2015).

150 A first reason related to modeling is that the influence of *LMA* on the optical properties modeled by
151 PROSPECT is defined by a single specific absorption coefficient (SAC), although various non-pigment
152 organic materials (cellulose, hemicellulose, lignin, proteins, starch) influence leaf optics individually
153 (Jacquemoud et al., 1996). Therefore, this single SAC assumes that the relative proportion of each of
154 these single constituents is constant among leaves, which may not be the case. Another reason may
155 be due to an imperfect modeling of light propagation within the leaf. From that perspective, Qiu et
156 al. (2018) proposed a refined version of PROSPECT (named PROSPECT-g) including an anisotropic-
157 scattering factor in order to improve the estimation of *LMA*, and developed an iterative inversion
158 procedure specifically dedicated to this model.

159 Experimental uncertainty should also be considered when discrepancies between measurements
160 and simulations are observed. Indeed, accurately measuring leaf optical properties remains
161 challenging despite the high performances of field and lab spectroradiometers, leading to possible
162 experimental bias which is usually unaccounted for. As an example, Merzlyak et al. (2004) reported
163 the difficulty to accurately measure leaf optical properties in the NIR domain due to incomplete
164 collection of the light leaving the highly scattering tissue. They proposed a correcting factor for

165 transmittance based on the hypothesis that leaf absorption in the NIR domain is negligible. For these
166 reasons, the relevance of systematically using the full spectral domain (especially the NIR domain)
167 can be questioned.

168 Finally, several authors suggested that classical least-squares inversion based on the use of leaf
169 reflectance and transmittance over the full spectral domain was suboptimal for physically-based
170 estimation of *LMA*, especially due to the lower influence of *LMA* on leaf optical properties in the
171 SWIR domain as compared to *EWT* (Colombo et al., 2008; Riano et al., 2005). More elaborated
172 inversion procedures have thus been proposed to improve *LMA* estimation. Some of them are
173 based on complex iterative procedures consisting in successively estimating different PROSPECT
174 parameters using unweighted merit functions computed over specific spectral domains (Qiu et al.,
175 2018 ; Li and Wang, 2011 ; Wang et al., 2015). When using the full spectral domain from 400 to 2500
176 nm, Sun et al. (2018) showed that *LMA* estimation based on PROSPECT inversion and an unweighted
177 merit function was more accurate when using only reflectance or only transmittance instead of
178 reflectance plus transmittance. When using bidirectional reflectance measurements, Li et al. (2018)
179 developed an approach (PROCWT) coupling PROSPECT with continuous wavelet transform in order
180 to suppress surface reflectance effects. PROCWT was shown to perform better than PROSPECT and a
181 simplified version of PROCOSINE (Jay et al., 2016) for the estimation of *LMA*.

182 All of these studies demonstrate the complexity of a direct estimation of *LMA* from leaf optical
183 properties using physically-based methods, and the difficulty to clearly identify the origin of current
184 limitations. In the case of data-driven methods, the estimation of *LMA* has seldom been investigated
185 comprehensively: training and test data are usually collected following a unique protocol specific to
186 a unique set of equipment and by the same team of operators. This means that possible
187 experimental biases due to protocol, equipment and/or operators may be embedded into the

188 resulting regression model, leading to poor generalization ability when applied to independent
189 datasets collected under different conditions or with different equipment.

190 The objective of this study is to assess the relative performances of physically-based and data-driven
191 approaches for the estimation of *LMA* and *EWT* based on leaf optical properties. Our working
192 questions are (1) what are the limitations of PROSPECT for *LMA* and *EWT* estimation, and is there
193 any solution to overcome these limitations, and (2) what is the generalization ability of data-driven
194 approaches when independent datasets are used for training and validation? We gathered six
195 datasets in temperate, tropical and boreal ecosystems, with joint measurements of broadleaf optical
196 properties, *LMA* and *EWT* (Section 2). Then, we designed specific protocols to address questions (1)
197 and (2), and to perform an objective comparison of their performances (Section 3). This includes the
198 selection of specific spectral information for PROSPECT inversion, and different strategies for the
199 sampling of the training dataset for ML algorithms. Section 4 presents the results obtained with the
200 different approaches, including a comparison of the validation with the six experimental datasets.
201 Finally, section 5 discusses the potential and current limitations of the approaches and section 6
202 provides a conclusion.

203

204 2. MATERIALS

205 a. Global description of the datasets

206 For this study, six datasets were collected over various ecoregions, ranging from tropical forests, to
207 temperate and boreal ecosystems (Table 1). LOPEX and ANGERS are publicly available and used in
208 many publications. HYTTIALA, ITATINGA, NOURAGUES and PARACOU are unpublished datasets.

209 - The ANGERS¹ dataset was collected in 2003 at INRA (Institut national de la recherche
210 agronomique) in Angers (France). It encompasses physical measurements and biochemical

¹ <http://opticleaf.ipgp.fr/index.php?page=database>

211 analyses collected over 43 species and varieties of woody and herbaceous plants. ANGERS was
212 used for the calibration of the SAC for chlorophylls, carotenoids and anthocyanins in the latest
213 versions of PROSPECT (Féret et al., 2017, 2008).

214 - The Leaf Optical Properties Experiment (LOPEX^{1,2}) dataset was collected in 1993 in Italy during a
215 campaign conducted at the Joint Research Centre (Ispra, Italy) (Hosgood et al., 1994). It
216 encompasses physical measurements and biochemical analyses collected over more than 50
217 species of woody and herbaceous plants, and has been widely used by the remote sensing
218 community (Bowyer and Danson, 2004; Féret et al., 2008; Mobasheri and Fatemi, 2013; Romero
219 et al., 2012). The full LOPEX dataset includes dry and fresh samples and was used for the
220 calibration of the SAC of *LMA* (Féret et al., 2008), as well as broadleaf and needleleaf samples.
221 However, only broadleaf samples were used in the current study, all fresh leaves except for one
222 set of five dry maize leaf samples.

223 - The HYYTIALA dataset was collected in July 2017 at the Hyytiälä Forestry Field Station in
224 Southern Finland in the frame of the Fluorescence Across Space and Time (FAST) campaign. This
225 station is located in the boreal belt and is dominated by mixed forest of Scots pine, Norway
226 spruce and silver birch. This dataset encompasses physical measurements and biochemical
227 analyses collected over various native and non-native broadleaf species located in the field
228 station.

229 - The ITATINGA dataset was collected in October 2015 as part of the IPEF-Eucflux project and
230 HYPERTROPIK project (TOSCA, CNES, France), from experimental *Eucalyptus* stands planted in
231 November 2009 near the University of São Paulo forestry research station at Itatinga
232 Municipality (São Paulo State, southeastern Brazil). ITATINGA includes sixteen genotypes and
233 four species of *Eucalyptus*, eventually with hybrids, provided by different forestry companies in

² <http://teledetection.ipgp.jussieu.fr/opticleaf/lopex.htm>

234 different regions of Brazil. For each genotype, leaves corresponding to various developmental
235 stages were collected, from juvenile to mature to senescent, and various locations within the
236 crown (shaded leaves from the lower part of the crown, leaves from mid crown and sunlit leaves
237 from the upper part of the crown). This dataset is the only genus-specific dataset. Hence, in spite
238 of the large variability in terms of developmental stages, the ranges of *LMA* and *EWT* show
239 significantly lower variability than those observed for the other datasets (Table 1). See Oliveira
240 et al. (2017) for more details.

241 - The NOURAGUES dataset was collected at the CNRS Nouragues experimental research station,
242 French Guiana, in September 2015, in the frame of the HYPERTROPIK project. This site is a
243 lowland Amazonian forest, protected since 1996 by a Natural Reserve status. This dataset
244 includes four to ten leaf samples from 38 emerging tropical tree species, collected from both
245 shaded and sunlit parts of the crown. The Nouragues station is also a pilot site for remote
246 sensing studies of tropical ecosystems (Réjou-Méchain et al., 2015).

247 - The PARACOU dataset was collected at the CIRAD-INRA Paracou experimental research station,
248 French Guiana, in September 2015 (HYPERTROPIK project). This dataset includes four to ten leaf
249 samples from 28 emerging tropical tree species, collected from both shaded and sunlit parts of
250 the crown. Paracou is located in coastal lowland Amazonian forest. Various experiments are
251 ongoing, including disturbance experiments, CO₂ flux experiments, fertilization and long-term
252 studies in forest dynamics and biodiversity.

253

254 b. Measurements of leaf optical properties

255 For all the samples, directional-hemispherical reflectance and transmittance (Schaepman-Strub et
256 al., 2006) of the upper surface of the leaves were measured with a spectroradiometer and an
257 integrating sphere in the visible (VIS), NIR and SWIR domains between 400 and 2500 nm. Here, we

258 used the infrared domain ranging from 900 to 2400 nm, due to the low influence of *LMA* and *EWT*
259 on leaf optical properties below 900 nm, and to the low signal-to-noise ratio (SNR) beyond 2400 nm.
260 All datasets shared the same protocol for the measurement of leaf optical properties, and included
261 spectral calibration for stray light in order to correct the imperfect collimation of the lamp beam as
262 well as compensation for the optical properties of the coating of the integrating sphere when
263 measuring leaf reflectance and transmittance (Asner et al., 2009; Carter and Knapp, 2001). The
264 datasets were collected by different operators, and using different devices. Despite efforts to share a
265 unique protocol for the acquisition of leaf optical properties, this diversity of operators, equipment
266 and conditions of acquisition, is a possible source of bias that we discuss here.

267

268 c. Measurements of *LMA* and *EWT*

269 The measurement of *EWT* and *LMA* shared the same protocol among experimental datasets. Leaf
270 samples were collected in the field, stored in a cooler and measured in an experimental facility
271 equipped with a precision scale and a drying oven. Minutes after measuring the leaf optical
272 properties, disks of fresh leaf material were sampled using a cork borer, and immediately weighted
273 using the precision scale to obtain *FW* (Eq. 2). The disks were then placed in a drying oven at 85°C
274 for at least 48 hours until constant mass was attained, and immediately weighted when out of the
275 oven in order to determine *DW* (Eq. 1 and Eq. 2) (Cornelissen et al., 2003; Pérez-Harguindeguy et al.,
276 2013). *EWT* and *LMA* were then computed based on Eq. 1 and Eq. 2.

277 Table 1 summarizes basic statistics and information for each dataset. *LMA* and *EWT* were
278 systematically measured for each sample in each dataset, except for the PARACOU dataset which
279 only includes *LMA* measurements. Similarly to optical properties, various sources of uncertainty may
280 have affected *EWT* and *LMA* measurements, including errors in the area sampled on leaf material
281 due to imperfect circular sampling disks, loss in water content between leaf optics measurements

282 and weighting of fresh mass, or rehydration between drying and weighting of dry mass. However,
 283 care was paid to standardize data collection, so as to minimize the influence of these possible biases.
 284 *EWT* and *LMA* show no correlation for ITATINGA, weak correlation for LOPEX, moderate correlation
 285 for HYTTIALA and NOURAGUES, and strong correlation for ANGERS. A moderate correlation of 0.44 is
 286 measured when pooling all samples together.

287

288 **Table 1.** Summary of the main properties of the experimental datasets. Basic statistics for each
 289 dataset (minimum and maximum value, mean and standard deviation) are given for *EWT* and *LMA*,
 290 as well as their correlation $r(EWT, LMA)$.

	ANGERS	LOPEX	HYTTIALA	ITATINGA	NOURAGUES	PARACOU
#Samples	308	330	96	415	262	272
#Species/genotypes	43 sp.	46 sp.	10 sp.	4 sp. /16 gt.*	38 sp.	28 sp.
<i>EWT</i> (mg.cm⁻²)						
Min – Max	4.40 – 34.00	0.29 – 52.48	3.68 – 23.73	2.20 – 20.20	3.20 – 38.10	N/A
Mean ± SD	11.47 ± 4.70	11.13 ± 6.97	9.16 ± 2.98	14.44 ± 2.09	11.73 ± 4.86	N/A
<i>LMA</i> (mg.cm⁻²)						
Min – Max	1.66 – 33.10	1.71 – 15.73	2.76 – 15.77	6.90 – 14.70	3.10 – 21.10	5.28 – 25.56
Mean ± SD	5.12 ± 3.53	5.29 ± 2.47	6.27 ± 3.04	10.24 ± 1.62	10.81 ± 3.89	12.32 ± 4.06
$r(EWT, LMA)$	0.72	0.28	0.40	0.03	0.51	N/A

291 * Four species from Eucalyptus genus, corresponding to sixteen genotypes

292

293 3. METHODS

294 a. PROSPECT model: general presentation

295 PROSPECT is based on the generalized plate model (Allen et al., 1969, 1970) and was initially
 296 developed by Jacquemoud and Baret (1990). This model simulates the leaf directional-hemispherical

297 reflectance and transmittance (Schaepman-Strub et al., 2006) with a limited number of input
298 biophysical and biochemical variables, including various absorbing compounds and a unique leaf
299 structure parameter, named N . Many versions have been developed since the first version, in order
300 to include more absorbing compounds (Féret et al., 2017, 2008; Jacquemoud et al., 1996) or to
301 adapt to specific conditions and leaf types, such as needle-shaped leaves (Malenovský et al., 2006).
302 In this study, we used the latest version of PROSPECT, named PROSPECT-D (Féret et al., 2017). As we
303 focused on leaf optical properties in the 900 – 2400 nm range, the capability of PROSPECT in terms
304 of separation of pigments was not critical as no pigment absorbs in this spectral domain, but the
305 refractive index differs from the one used on PROSPECT-5 (Féret et al., 2008). Brown pigments were
306 not retrieved during the inversion, as including them showed no significant difference in the results
307 obtained for any of the strategies tested here.

308 The N parameter corresponds to the number of uniform compact plates separated by $N - 1$ air
309 spaces. The value of N represents the complexity of the leaf internal structure, with low N values
310 corresponding to moderate complexity such as in monocots, and higher N values corresponding to
311 higher complexity, a characteristic of dicots. To date, no protocol exists to experimentally estimate
312 N from leaf samples, other than using leaf optical properties. N influences leaf scattering and shows
313 negligible impact on leaf absorption: increasing N values increase reflectance and decrease
314 transmittance, and N shows particularly strong effects in domains with low absorption, such as the
315 NIR domain. Recently, Qiu et al. (2018) found an extremely strong correlation between N and the
316 ratio between reflectance and transmittance on simulated data.

317 PROSPECT can be run in forward or inverse mode. The forward mode aims at simulating leaf optical
318 properties based on a full set of biophysical and biochemical properties (leaf chemistry and N). The
319 inverse mode aims at identifying the optimal set of biophysical and biochemical properties that
320 minimize a merit function (or goodness-of-fit criterion) based on a comparison between measured

321 and simulated leaf optics. A common inversion procedure is based on the numerical minimization of
 322 the sum of weighted square errors over all spectral bands available. The corresponding merit
 323 function M is expressed as follows when using both reflectance and transmittance:

324

$$M(N, \{C_i\}_{i=1:p}) = \sum_{\lambda=\lambda_1}^{\lambda_n} [W_{R,\lambda} \times (R_\lambda - \hat{R}_\lambda)^2 + W_{T,\lambda} \times (T_\lambda - \hat{T}_\lambda)^2] \quad \text{Eq. 3}$$

325

326 with N the leaf structure parameter, p the number of chemical constituents accounted for by
 327 PROSPECT and retrieved during the inversion, C_i the biochemical content per leaf surface unit for
 328 constituent i , λ_1 and λ_n the first and last wavebands investigated for inversion, R_λ and T_λ the
 329 experimental reflectance and transmittance measured at waveband λ , \hat{R}_λ and \hat{T}_λ the reflectance and
 330 transmittance simulated by PROSPECT with $\{N, \{C_i\}_{i=1:p}\}$ as input variables, $W_{R,\lambda}$ the weight
 331 applied to the squared difference between experimental and simulated reflectances, and $W_{T,\lambda}$ its
 332 equivalent for transmittance. Eq. 3 can be used to estimate the full set of input variables, or a limited
 333 subset if prior information or arbitrary value is set for some variables.

334 b. Estimation of *EWT* and *LMA* through iterative optimization

335 The large majority of the studies focusing on leaf scale model inversions through iterative
 336 optimization used Eq. 3 with unweighted merit function over the full spectral domain available
 337 ($W_{R,\lambda} = W_{T,\lambda} = 1$). This merit function provides accurate estimates of leaf pigments and *EWT* (Féret
 338 et al., 2017; Jacquemoud et al., 1996; Newnham and Burt, 2001), but several studies reported poor
 339 results for *LMA* estimation (Féret et al., 2008; Riano et al., 2005). Colombo et al. (2008) used an
 340 alternative weighting, with $W_{R,\lambda} = (R_\lambda)^{-2}$ and $W_{T,\lambda} = (T_\lambda)^{-2}$, which is otherwise unused in the
 341 literature when inverting leaf models, and not so common when inverting canopy models (Baret and
 342 Buis, 2008). In practice, implementing such a merit function requires precaution as high sensor noise

343 (in particular in the SWIR domain) may result in close-to-zero reflectance and transmittance, leading
344 to exaggerated importance of the corresponding spectral bands. This merit function then needs to
345 be adapted to exclude these spectral bands. Colombo et al. (2008) reported fair performances of this
346 merit function for the estimation of *EWT*, but poor performances for *LMA*. However, the SWIR
347 domain beyond 1600 nm was not measured for their study, in spite of its importance for the
348 estimation of *LMA* (Asner et al., 2011, 2009; le Maire et al., 2008). Therefore a fair comparison
349 between this merit function and the unweighted merit function including the full spectral range is
350 required.

351 As mentioned in the introduction, *LMA* estimation could also be improved by focusing on optimal
352 spectral ranges (Li and Wang, 2011; Qiu et al., 2018; Wang et al., 2015). This amounts to choosing
353 the weights such that $W_{R,\lambda} = W_{T,\lambda} = 1$ in the considered range, and $W_{R,\lambda} = W_{T,\lambda} = 0$ elsewhere.
354 Note that such a procedure is relatively straightforward and could potentially be applied to the
355 canopy scale in a similar way.

356 In this study, three inversion procedures were applied to the six independent experimental datasets,
357 and their relative performances were compared. These inversion procedures correspond to “one-
358 step” procedures, aiming at estimating *EWT*, *LMA* and *N* simultaneously from both reflectance and
359 transmittance:

360 - *Iterative optimization 1 (IO1)* uses an unweighted merit function ($W_{R,\lambda} = W_{T,\lambda} = 1$) with
361 reflectance and transmittance defined from 900 nm to 2400 nm.

362 - *Iterative optimization 2 (IO2)* uses a weighted merit function as defined by Colombo et al. (2008)
363 ($W_{R,\lambda} = (R_\lambda)^{-2}$ and $W_{T,\lambda} = (T_\lambda)^{-2}$) with reflectance and transmittance defined from 900 nm to
364 2400 nm.

365 - *Iterative optimization 3 (IO3)* uses a weighted merit function defined by $W_{R,\lambda} = W_{T,\lambda} = 1$ over
366 an optimal contiguous spectral domain $[\lambda_1, \lambda_n]$ defined between 900 and 2400 nm, and

367 $W_{R,\lambda} = W_{T,\lambda} = 0$ elsewhere. This optimal spectral domain is adjusted in the present study and is
368 the same for both reflectance and transmittance, and for all experimental datasets.

369 In the case of *IO3*, the exhaustive comparison of all combinations of spectral domains or spectral
370 bands is computationally too demanding and extremely inefficient given the strong correlations
371 between neighboring spectral domains. In order to reduce the computational cost, we focused on
372 contiguous spectral domains defined by partitioning the initial spectral domain into 15 evenly-sized
373 segments of 100 nm from 900 to 2399 nm. The choice of 100 nm segments is driven by constraints in
374 terms of computation and by the ability to identify the main absorption features of *EWT* and *LMA*
375 individually. The performances of PROSPECT inversion for the estimation of *LMA* and *EWT* were
376 tested with all continuous spectral domains that can be generated from these 15 spectral segments,
377 leading to 120 continuous segments. Finally, the spectral domain leading to the minimum RMSE
378 averaged for all experimental datasets and for the estimation of both *LMA* and *EWT* from
379 PROSPECT inversion was selected and defined as the optimal spectral range used in *IO3*.

380 For *IO1*, *IO2* and *IO3*, *N*, *EWT* and *LMA* were simultaneously estimated using a constrained
381 nonlinear optimization algorithm, i.e., the Sequential Quadratic Programming algorithm
382 implemented within the Matlab function *fmincon*. The lower bounds selected for the three
383 parameters to be optimized were defined to respect the condition of strict positivity and include
384 minimum values observed for experimental data, whereas the upper bounds were set in order to
385 include the maximum values observed for experimental data, with significant margins: *EWT* values
386 were investigated between 0.01 and 80 mg.cm⁻²; *LMA* values were investigated between 0.01 and
387 40 mg.cm⁻²; *N* values were investigated between 0.5 and 4. No correlation constraints between
388 *EWT* and *LMA* were included in the inversion procedure, since such correlation was not systematic
389 between datasets.

390

391 c. Data-driven estimation of *EWT* and *LMA*

392 The performances of data-driven methods inherently depend on the training data. In most cases,
393 these performances are reported after splitting an experimental dataset into training and validation
394 subsets, and the resulting regression models are not validated on fully independent datasets. In the
395 perspective of operational applications, this raises the question of the possibility to share regression
396 models adjusted with ML algorithms on public experimental datasets, and to use leaf spectroscopy
397 operationally with no destructive measurements required to adjust dataset-specific regression
398 models. With increasing use of machine learning, software packages including already trained
399 regression models may be shared the same way statistical models derived from spectral indices have
400 been proposed in the scientific literature (Féret et al., 2011). We want to answer the following
401 questions related to data-driven methods: do regression models trained with one or several
402 experimental datasets perform well when applied on independent datasets, or should training data
403 systematically include samples from the validation dataset? To answer these questions, three
404 strategies for the composition of a training dataset were tested, and the performances of data-
405 driven methods were compared with PROSPECT inversions:

- 406 - *Training sampling 1 (TS1)*: A single dataset was used as training data and the regression model
407 was then applied on each of the remaining datasets.
- 408 - *Training sampling 2 (TS2)*: All but one experimental datasets were used as training data, and the
409 regression model was then applied on the remaining dataset.
- 410 - *Training sampling 3 (TS3)*: All experimental datasets were pooled into a single one, and 300
411 samples (comparable in size to individual datasets) were randomly selected for training.
412 Validation was then performed on the remaining samples (1668 samples for *LMA*, and 1396
413 samples for *EWT*), and performances (in terms of RMSE) were evaluated per individual dataset
414 and globally. In each case, to account for possible sampling bias, random sampling of training

415 dataset was repeated 20 times and the distribution of RMSE values across all samplings was
416 calculated.

417 Here, these three strategies used to define the training dataset were used with support vector
418 machine (SVM) regression algorithm corresponding to the *Matlab* implementation of the *LibSVM*
419 library (Chang and Lin, 2011). Reflectance and transmittance measurements from 900 to 2400 nm
420 were stacked in a unique vector, resulting in $n_\lambda = 3002$ predictor spectral variables for each sample.
421 Reflectance and transmittance were scaled between 0 and 1 for each spectral band, as well as leaf
422 chemical constituent of interest (*LMA* and *EWT*). The radial basis function (RBF) kernel was
423 selected, which implies optimizing two free parameters, C and γ . C is a cost parameter used to trade
424 error penalty for stability and common to any SVM model. γ is specific to RBF kernels and it
425 corresponds to the inverse of the radius of influence of samples selected by the model as support
426 vectors. The C and γ parameters were optimized using an exhaustive grid search
427 ($C \in [10^{-2}; 10^{-1}; \dots; 10^{+2}]$, $\gamma \in [10^{-5}; 10^{-4}; \dots; 10^{+1}]$) in order to include the default values
428 recommended by Chang and Lin (2011) and a five-fold cross validation over the training data for
429 each combination of C and γ . The optimal C and γ values were then used with the full training data
430 to adjust a regression model.

431

432 4. RESULTS

433 This section is divided into three subsections. The first subsection aims at identifying the optimal
434 spectral domain to be used with *IO3*. This first section is a prerequisite to the second section, which
435 then focuses on the comparison between the three types of iterative optimization, and the two
436 types of training samplings based on the integrality of experimental datasets, *TS1* and *TS2*. Finally,
437 the third section compares the performances of *TS3*, which is based on a random sampling among all

438 experimental datasets, with the performances of *IO3* and *TS2*, when the validation samples are
439 identical to those used in *TS3*.

440 a. Influence of spectral domain used for the estimation of *EWT* and *LMA* with
441 PROSPECT inversion (optimization of *IO3* method)

442 Figure 1 and Figure 2 show the results obtained for the estimation of *EWT* and *LMA*, respectively,
443 when inverting PROSPECT over each dataset and each of the 120 spectral domains defined in Section
444 3.b with the *IO3* method. For the sake of comparison, for each dataset, the RMSE was normalized by
445 the RMSE obtained when using the spectral information from 900 to 2400 nm, and this normalized
446 RMSE (NRMSE) was expressed as a percentage. In the case of *EWT*, the optimal spectral domain
447 excluded the NIR domain under 1300 nm for all datasets, but no unique optimal spectral domain
448 common to each dataset could be identified. The relative improvement induced by the reduction of
449 the spectral domain was also strongly dataset-dependent: NRMSE was reduced by 23 % (LOPEX) to
450 56 % (NOURAGUES).

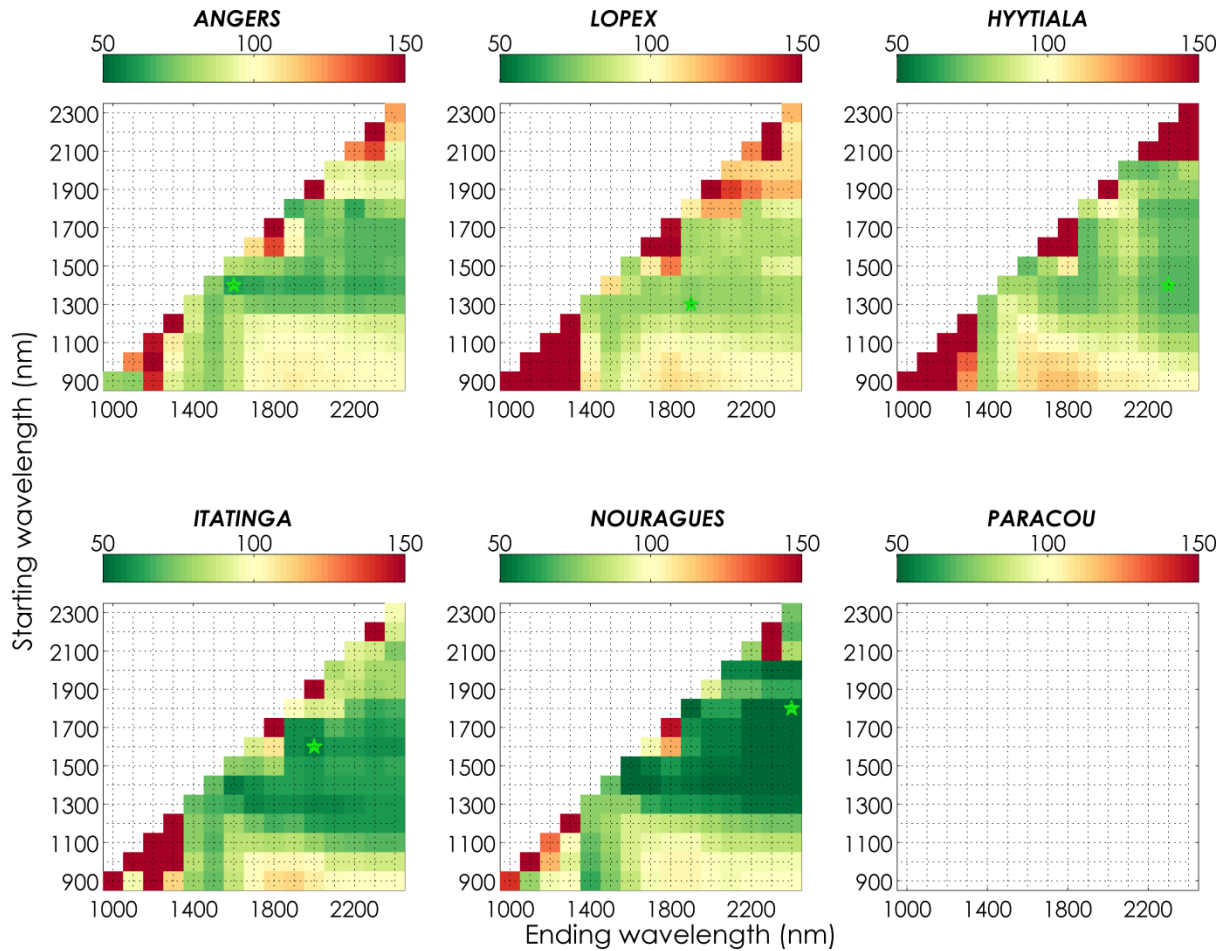


Figure 1. Normalized *RMSE* (*NRMSE*, in %) obtained for *EWT* with PROSPECT inversion method *IO3* over each dataset and each reduced spectral domains bounded by a starting wavelength λ_1 (y-axis) and an ending wavelength λ_2 (x-axis). The normalization is specific to each dataset based on the performances of *IO1* (*NRMSE*=100%, lower right corner). The green star indicates the spectral segment producing the best results.

451

452 In the case of *LMA*, both optimal spectral domain and relative improvement or degradation showed
 453 stronger consistency among datasets than for *EWT* (Figure 2). For all datasets, excluding
 454 information from 1500 nm and beyond led to strong degradations of the performances. In the case

455 of LOPEX and HYYTIALA, estimation of *LMA* could be improved only when using spectral domains
456 with ending wavelength between 2100 and 2400 nm, except when using a narrow spectral domain
457 from 1600 to 1800 nm. For the four other datasets, extended spectral combinations led to improved
458 *LMA*, as most of the combinations excluding the domain from 900 to 1200 nm led to improved
459 estimation of *LMA*, except when using a reduced spectral domain ranging from 1800 to 2100 nm
460 only, which corresponds to one of the main absorption features of water. Overall, the optimal
461 spectral range excluded the NIR domain and included spectral information until 2400 nm for all
462 datasets. The relative improvement induced by the selection of an optimal specific for each dataset
463 ranged from 60 (ITATINGA) to 67 % (NOURAGUES).
464

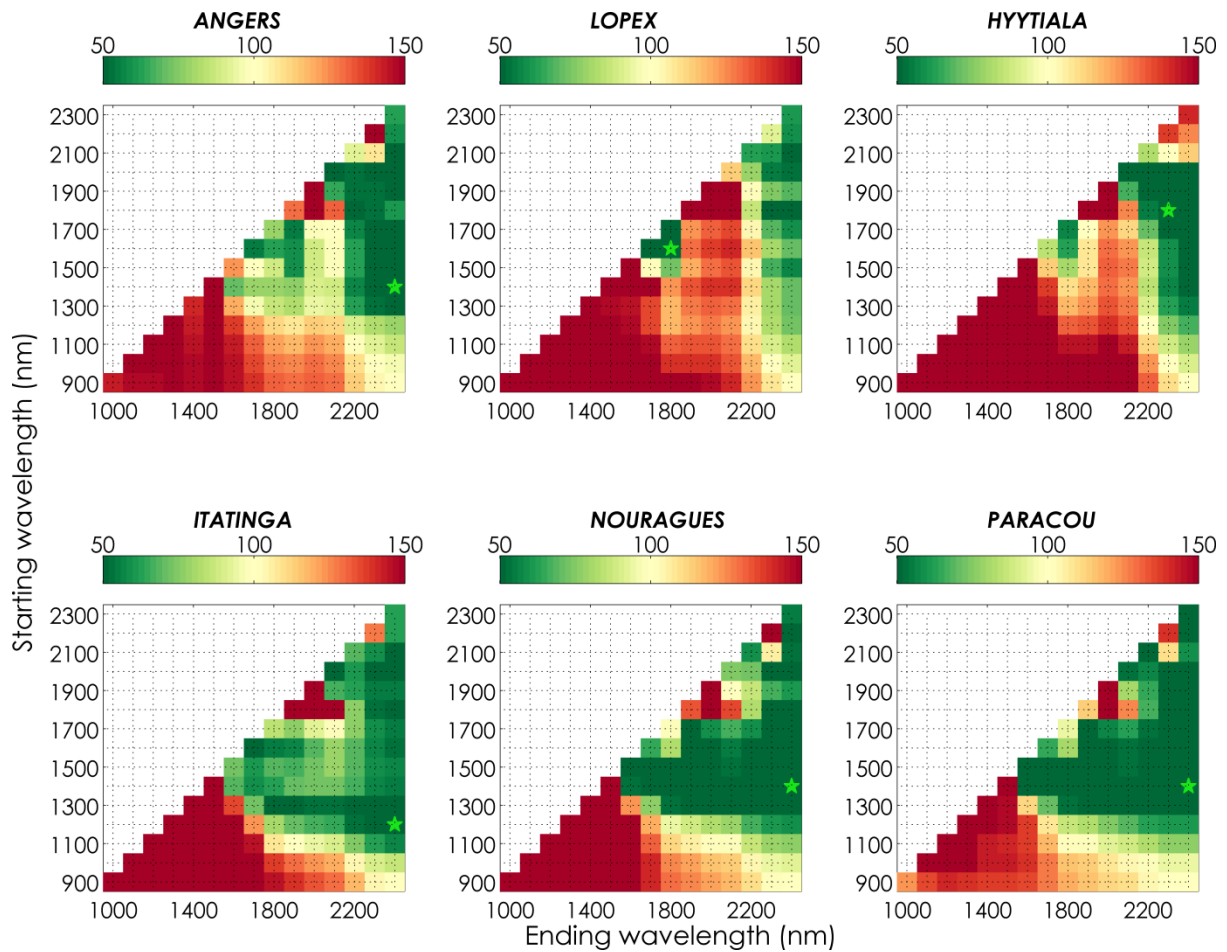


Figure 2. Normalized *RMSE* (NRMSE, in %) obtained for *LMA* estimation with PROSPECT inversion method *IO3*, over each dataset and each reduced spectral domains bounded by a starting wavelength λ_1 (y-axis) and an ending wavelength λ_2 (x-axis). The normalization is specific to each dataset based on the performances of *IO1* (NRMSE=100%, lower right corner). The green star indicates the spectral segment producing the best results.

465

466 These figures provide a visual representation of the spectral domains leading to improved or
 467 decreased performances compared to full spectral information. They confirm that selecting the
 468 appropriate spectral information during inversion strongly influences for the estimation of leaf
 469 constituents.

470 Figure 3 provides NRMSE for the estimation of *EWT* and *LMA* averaged over all datasets, and
 471 confirms suboptimal performances obtained when using NIR information only. Overall, the spectral
 472 domain ranging from 1700 to 2400 nm was found to be optimal when estimating *EWT* and *LMA*
 473 simultaneously (mean NRMSE was reduced by 33% for *EWT* and by 55 % for *LMA*), and was used
 474 hereafter within the *IO3* method.
 475

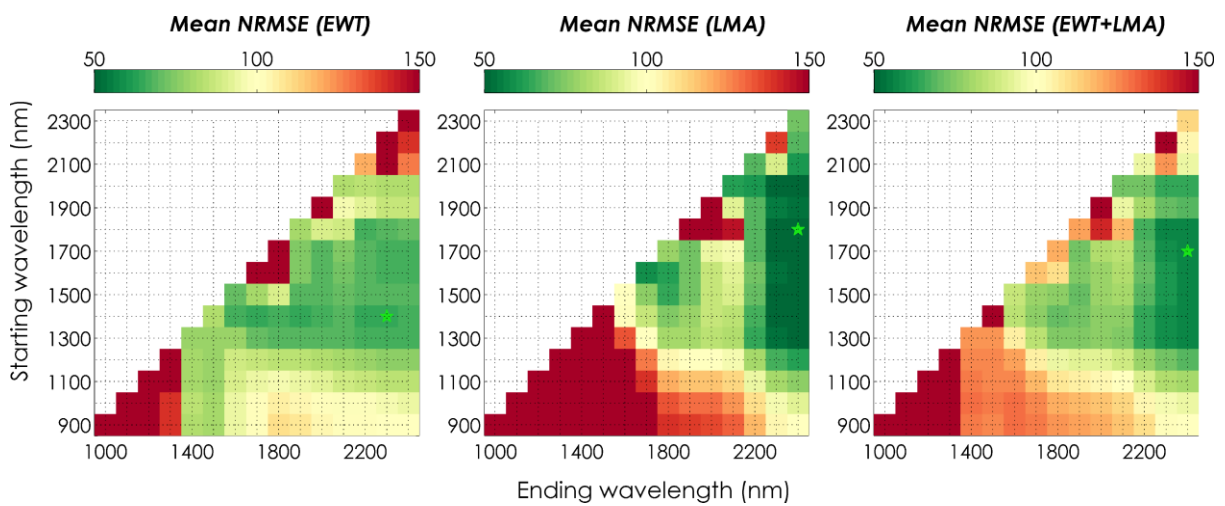


Figure 3. Mean normalized RMSE values (NRMSE, in %) obtained for the estimation of *EWT* (left), *LMA* (center), and both constituents (right), after PROSPECT inversion over all experimental datasets pooled and each of the 120 spectral domains defined in Section 3.b. The green star indicates the spectral segment producing the best results.

476

477 b. Comparison of PROSPECT inversion methods and ML algorithms for the estimation
 478 of *LMA* and *EWT*: training ML with independent datasets

479 The performances obtained for the estimation of *EWT* when using *TS1* and *TS2* for ML regression,
 480 and *IO1*, *IO2* or *IO3* (with the 1700 – 2400 nm spectral range) for PROSPECT inversion are reported in
 481 Table 2. Overall, *IO2* and *IO3* produced the most consistent results, systematically outperforming the

482 other methods. ML regressions performed particularly poorly compared to *IO2* and *IO3*, and *TS2* led
 483 to the better results than *TS1* (except form HYYTIALA). *TS1* led to very inconsistent results, with
 484 175% increase compared to *IO2* and *IO3* on average, and up to 500% increase in RMSE compared to
 485 PROSPECT inversion *IO2* when estimating *EWT* from ITATINGA after training with LOPEX.

486

487 **Table 2.** RMSE values (in $\text{mg}\cdot\text{cm}^{-2}$) obtained for the estimation of *EWT* with SVM and training
 488 strategies *TS1* and *TS2*, and with *IO1*, *IO2* and *IO3*. For each column (validation dataset), the
 489 minimum RMSE is indicated in bold, and colors correspond to the level of performances, from green
 490 color for minimum RMSE to red color for maximum RMSE.

Method		Valid					
		ANGERS	LOPEX	HYYTIALA	ITATINGA	NOURAGUES	PARACOU
Train							
<i>TS1</i>	ANGERS	-	4.82	1.90	3.31	2.49	-
	LOPEX	3.14	-	3.23	6.73	2.32	-
	HYYTIALA	3.79	5.40	-	2.84	3.92	-
	ITATINGA	3.38	5.82	3.03	-	3.43	-
	NOURAGUES	2.54	5.04	3.15	2.47	-	-
	PARACOU	-	-	-	-	-	-
<i>TS2</i>	All but 1	2.47	4.54	2.68	2.08	2.10	-
<i>IO1</i>	PROSPECT	2.07	2.03	1.72	1.93	3.44	-
<i>IO2</i>	PROSPECT	1.48	1.68	1.44	1.13	1.21	-
<i>IO3</i>	PROSPECT	1.41	1.70	1.21	1.20	1.66	-

491

492 Figure 4 provides scatterplots for the results showed in Table 2 and corresponding to *IO1*, *IO2*, *IO3*
 493 and SVM regression with sampling strategy *TS2*. Overall, *IO2* showed the best performances for the
 494 estimation of *EWT*, and SVM regression produced the lowest performances, mainly because of the
 495 strong error obtained for extreme values on LOPEX.
 496

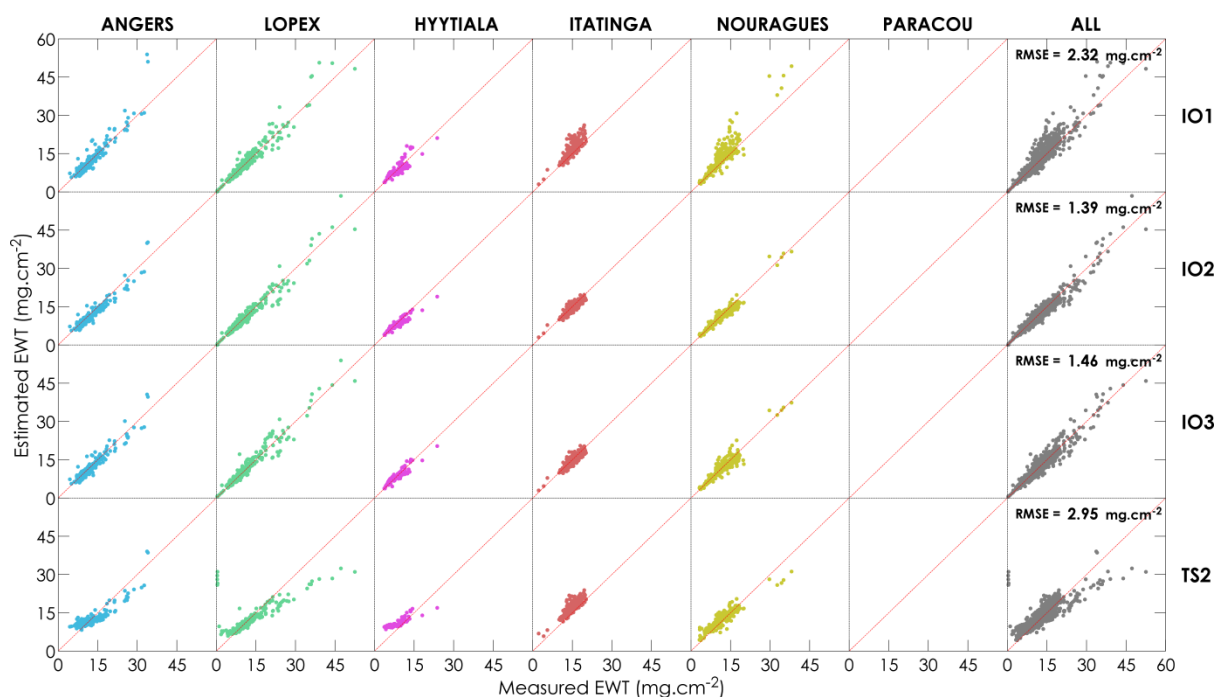


Figure 4. *EWT* estimation results obtained using PROSPECT inversion (*IO1*, *IO2*, *IO3*) and ML regression (training sampling *TS2*).

497
 498 The performances obtained for the estimation of *LMA* when using training samplings *TS1* and *TS2*
 499 for ML regression, and *IO1*, *IO2* or *IO3* for PROSPECT inversion are reported in Table 3. *IO3*
 500 outperformed the other methods for all datasets except HYTTIALA and ITATINGA: *IO2* slightly
 501 outperformed *IO3* for ITATINGA only and *TS2* outperformed *IO3* for HYTTIALA and ITATINGA.
 502 However, the difference in RMSE between *IO3* and the optimal method remained less than 20% for
 503 these two datasets. The relative performances obtained with *IO1* and *IO2* differed among datasets:

504 while using *IO2* led to significantly improved estimation of *LMA* compared to *IO1* for five datasets
 505 (from a 26% decrease in RMSE for LOPEX to more than 50% for ITATINGA, NOURAGUES and
 506 PARACOU), and slightly degraded estimation compared to *IO3* for four datasets, the performances
 507 obtained for HYYTIALA were degraded by more than 75% compared to *IO1*, with systematic strong
 508 overestimation (Figure 5). On the other hand, the RMSE corresponding to estimation of *LMA* using
 509 *IO3* decreased by 60% compared to *IO1*. ML regression trained with *TS2* performed better than *IO1*
 510 overall but was outperformed by *IO2* and *IO3*. As for *EWT*, ML trained with *TS1* led to very
 511 inconsistent results, and was strongly outperformed by *IO2*, *IO3* and ML regressions trained with
 512 strategy *TS2* in most cases.

513

514 **Table 3.** RMSE values (in mg.cm⁻²) obtained for the estimation of *LMA* with SVM and training
 515 samplings *TS1* and *TS2*, and with *IO1*, *IO2* and *IO3*. For each column (validation dataset), the
 516 minimum RMSE is indicated in bold, and colors correspond to the level of performances, from green
 517 color for minimum RMSE to red color for maximum RMSE.

Method		Valid					
		ANGERS	LOPEX	HYYTIALA	ITATINGA	NOURAGUES	PARACOU
Train							
<i>TS1</i>	ANGERS	-	4.91	2.49	3.73	2.76	2.70
	LOPEX	2.92	-	2.18	4.33	4.85	5.86
	HYYTIALA	2.51	2.47	-	3.19	3.32	4.00
	ITATINGA	6.27	5.57	5.08	-	3.86	4.50
	NOURAGUES	4.04	4.82	3.74	1.40	-	2.21
	PARACOU	2.96	3.96	2.30	1.25	2.11	-
<i>TS2</i>	All but 1	2.31	4.06	1.33	1.23	2.14	2.41

<i>IO1</i>	PROSPECT	2.48	3.36	3.49	2.60	3.95	4.75
<i>IO2</i>	PROSPECT	1.24	2.48	6.12	1.20	1.71	2.25
<i>IO3</i>	PROSPECT	0.93	1.99	1.52	1.44	1.59	1.73

518

519 Figure 5 provides scatterplots for the results showed in Table 3 and corresponding to *IO1*, *IO2*, *IO3*
520 and SVM regression with training sampling *TS2*. Overall, *IO3* produced the most accurate estimation
521 of *LMA*. *IO2*, *IO3* and *TS2* respectively resulted in 33%, 55% and 27% decreases in RMSE for the
522 estimation of *LMA* when compared to *IO1*.

523

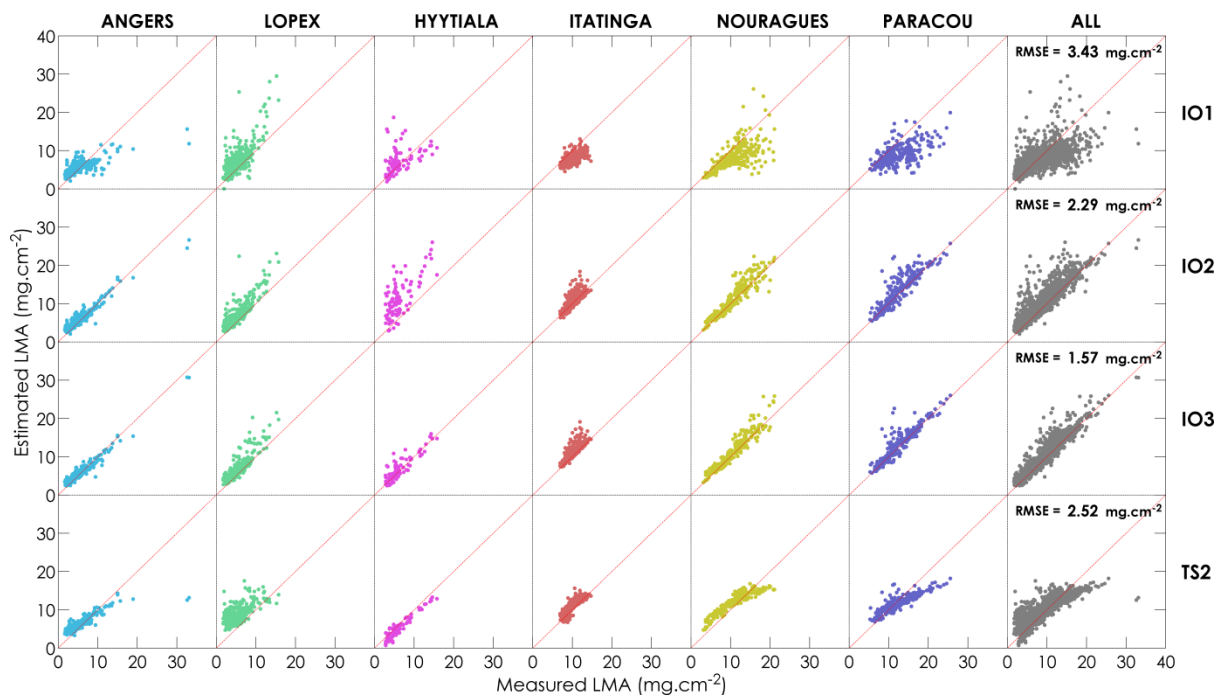


Figure 5. *LMA* estimation results obtained using PROSPECT inversion (*IO1*, *IO2*, *IO3*) and SVM regression (training sampling *TS2*).

524

525 c. Comparison of PROSPECT inversion methods and ML algorithms for the estimation
526 of *LMA* and *EWT*: training ML with pooled datasets

527 Table 4 and Table 5 summarize the performances of SVM regression for the estimation of *EWT* and
528 *LMA* when *TS3* is selected as training strategy (i.e. all dataset are pooled together and 300
529 calibration samples are randomly selected). The performances corresponding to *IO3* and *TS2* were
530 computed for the same validation samples as with *TS3* for each of the 20 repetitions in order to
531 ensure fair comparison.

532 The mean performances reported in Table 4 and Table 5 were very similar to those reported in Table
533 2 and Table 3 for both *IO3* and *TS2*, which means that *IO3* systematically outperformed *TS2* on
534 individual datasets, except for the estimation of *LMA* for HYTTIALA and ITATINGA. *TS3*
535 outperformed *TS2* in most cases for the estimation of both *EWT* and *LMA*. Still, *TS3* was
536 outperformed by *IO3* when estimating *EWT*, the overall RMSE increasing by 44% (and by 99% when
537 using *TS2*). When estimating *LMA*, *TS3* and *IO3* showed very similar overall performances, with less
538 than 6% increase of RMSE for *TS3* when compared to *IO3*. *IO3* and *TS3* showed very similar average
539 RMSE for LOPEX, HYTTIALA and NOURAGUES, *TS3* showed higher RMSE for ANGERS and PARACOU,
540 and lower RMSE for ITATINGA. However, the standard deviations associated with these
541 performances highlight the strong effect of training and validation samplings on the performances of
542 the ML algorithm: the standard deviation computed over 20 repetitions was 5 to 20 times higher for
543 *TS3* than *IO3* when estimating *EWT*, while it was 2.5 to 10 times higher when estimating *LMA*. The
544 standard deviations related to the performances of *TS2* were generally similar to those obtained for
545 *IO3*, suggesting that the strong differences in performance between regression models were induced
546 by the selection of the training samples.

547

548 **Table 4.** Mean RMSE and standard deviation of RMSE (both in $\text{mg}\cdot\text{cm}^{-2}$) of the estimation of *EWT*
 549 using SVM regression (*TS2* and *TS3*) and PROSPECT inversion (*IO3*) on the validation samples used for
 550 *TS3*. Best mean performances are indicated in bold.

	ANGERS	LOPEX	HYTTIALA	ITATINGA	NOURAGUES	PARACOU	Total
<i>TS3</i>	1.76±0.24	2.77±0.47	2.08±0.37	1.64±0.33	2.18±0.37	-	2.12±0.26
<i>TS2</i>	2.47±0.04	4.55±0.28	2.66±0.07	2.08±0.04	2.1±0.05	-	2.97±0.10
<i>IO3</i>	1.43±0.04	1.70±0.07	1.21±0.04	1.21±0.02	1.65±0.05	-	1.47±0.02

551
 552 **Table 5.** Mean RMSE and standard deviation of RMSE (both in $\text{mg}\cdot\text{cm}^{-2}$) of the estimation of *LMA*
 553 using SVM regression (*TS2* and *TS3*) and PROSPECT inversion (*IO3*) on the validation samples used for
 554 *TS3*. Best mean performances are indicated in bold (differences in mean RMSE < 1% are considered
 555 equivalent).

	ANGERS	LOPEX	HYTTIALA	ITATINGA	NOURAGUES	PARACOU	Total
<i>TS3</i>	1.70±0.28	1.98±0.56	1.56±0.22	1.12±0.29	1.59±0.19	2.01±0.18	1.64±0.18
<i>TS2</i>	2.24±0.21	4.05±0.06	1.33±0.04	1.23±0.02	2.13±0.03	2.43±0.05	2.31±0.05
<i>IO3</i>	0.92±0.03	2.00±0.07	1.54±0.08	1.45±0.04	1.58±0.06	1.77±0.07	1.54±0.03

556
 557 5. DISCUSSION

558 a. Differences in performances among merit functions
 559 Our study shows that *IO1*, the most commonly used merit function, is actually outperformed by a
 560 less common merit function (*IO2*) when estimating *EWT* and *LMA* from PROSPECT inversion using
 561 reflectance and transmittance in the NIR/SWIR domain (900-2400 nm). These results are in
 562 agreement with the results obtained when investigating the optimal spectral domain to be used with

563 *IO3*: Figure 3 shows that, in most cases, selecting a spectral domain including NIR information leads
564 to suboptimal estimation of both *EWT* and *LMA*. Therefore, the application of a weight inversely
565 proportional to the square of the reflectance and transmittance (*IO2*) reduce the importance of
566 spectral domains showing higher reflectance and transmittance values such as the NIR domain. The
567 improvement is particularly strong for the estimation of *LMA*, as reported in Figure 3. The
568 particularly low performances obtained for the estimation of *LMA* on HYYTIAA were also
569 investigated. The leaf optical properties measured for this dataset showed low SNR, particularly in
570 the SWIR domain for wavelengths of 2300 nm and beyond. The estimation of *LMA* with *IO2* was
571 strongly improved on this dataset when applying a Savitzky-Golay smoothing filter and restricting
572 the spectral domain from 1700 to 2300 nm. The exclusion of the spectral domain beyond 2300 nm
573 was responsible for the strongest improvement. Finally, the RMSE obtained for HYYTIAA when using
574 the merit function used in *IO2* and these preprocessing reached 1.97 mg.cm^{-2} , which is still 30%
575 higher than the RMSE obtained with *IO3*. Therefore using *IO2* is strongly discouraged when the
576 signal to noise ratio of leaf optical properties is not sufficient, while *IO3* based on the 1700-2400 nm
577 spectral range appears to be reliable even with low SNR.

578

579 b. Physical interpretation of the performances obtained with PROSPECT inversion

580 As highlighted in the previous section, the SNR of leaf optical properties can become a strong
581 limitation when estimating leaf constituents using PROSPECT inversion if the spectral domain and
582 merit functions are not carefully chosen. However, this SNR is not the main limiting factor explaining
583 the poor performances of *IO1* for the estimation of *LMA* and its suboptimal performances for the
584 estimation of *EWT*. Indeed, the NIR domain is theoretically characterized by a higher signal to noise
585 ratio for leaf material but still appears to be the main limitation for an accurate estimation of these

586 leaf constituents. Therefore, we attempt here to list possible explanations for such poor
587 performances.

588 i. Predominant water absorption

589 The main reason cited to explain the poor retrieval of *LMA* is the predominant water absorption in
590 the SWIR domain. Indeed, Figure 3 **Erreur ! Source du renvoi introuvable.** shows that *LMA* is poorly
591 estimated when the spectral domains used for inversion mainly include domains with strong water
592 absorption, such as the domain from 1800 to 2100 nm. However Figure 3 also shows that *LMA* can
593 still be estimated accurately even if most of the spectral information corresponds to domains with
594 predominant water absorption. Our results show that the main limitation with *IO1* is actually caused
595 by the NIR domain between 900 and 1300 nm: most of the spectral domains excluding such
596 wavebands resulted in improved estimation of *LMA*. The 900-1300 nm range does not show
597 predominant water or dry matter absorption, so the poor retrieval of *LMA* cannot be explained by
598 absorption features hidden by water absorption or any other constituent.

599 ii. Approximations of PROSPECT

600 As any model, PROSPECT is based on a number of approximations. Although some of these
601 approximations are possible sources of inaccuracy in specific situations, they guarantee good overall
602 performances given a minimum number of descriptors of leaf biophysical properties. Model
603 discrepancies in the simulation of leaf optical properties may be explained by inaccurate physical
604 description at three levels: surface effects, volume scattering and volume absorption.

605 Surface effects strongly depend on the presence of waxes or trichomes, and Barry and Newnham
606 (2012) reported how epicuticular waxes affect PROSPECT inversion. Surface effects mostly influence
607 leaf reflectance in the domains characterized by strong absorption where the leaf reflectance is
608 minimum (Bousquet et al., 2005; Jay et al., 2016). In the NIR/SWIR spectral range, these domains
609 mainly depend on water absorption. The sensitivity analysis performed by Jay et al. (2016) with

610 similar *EWT* values showed that surface effects have the largest influence beyond 1800 nm, this
611 domain being close to the one leading to optimal PROSPECT inversion results with *IO3* (1700-2400
612 nm). Such a result thus tends to indicate that surface effects had a limited detrimental influence on
613 estimation performance.

614 Volume scattering is modeled by multiple factors in PROSPECT, including leaf structure with the *N*
615 parameter, and the refractive index. The unique value of the refractive index is a well-identified
616 simplification of PROSPECT, as it does not agree with the Kramers-Kronig relations stating that the
617 real (refractive index) and imaginary (absorption coefficient) parts of the complex refractive index of
618 a medium are physically linked (Lucarini et al., 2005). Qiu et al. (2018) developed PROSPECT-g, a
619 modified version of PROSPECT including an additional wavelength-independent factor specific to
620 each leaf and aiming at representing first-order effects of anisotropic scattering, which are not
621 included through the *N* structural parameter of the original PROSPECT model. They also proposed a
622 multistage inversion to be used with PROSPECT-g. This inversion procedure may strongly increase
623 computing time, and the applicability of PROSPECT-g inversion at the canopy scale does not seem
624 straightforward as additional parameters may increase the ill-posedness of canopy models such as
625 PROSAIL (Jacquemoud et al., 2009). However, they reported promising results, including improved
626 estimation of *LMA* and improved simulation of both reflectance and transmittance in the NIR
627 domain when compared to PROSPECT-5.

628 Volume absorption is defined by the SACs which are adjusted based on experimental data during the
629 calibration of PROSPECT (Féret et al., 2008, 2017). We attempted a recalibration of the SAC for *LMA*
630 in order to reduce the inaccuracies observed between experimental and simulated data, and
631 improve the estimation of *LMA*. This did not lead to any improvement when including the NIR
632 domain. Moreover, the incorrect definition of the SAC corresponding to *LMA* would lead to
633 systematic underestimation or overestimation of absorption when running PROSPECT in direct

634 mode. However, the analysis of the residuals between measured leaf optical properties and their
635 simulated counterparts obtained with PROSPECT in direct mode did not result in systematic errors
636 (results not shown). The SAC corresponding to *LMA* in PROSPECT integrates the optical influences of
637 various organic constituents, which may also lead to inaccuracies if leaf samples include strong
638 variations in stoichiometry. However, the data required to test this possible source of inaccuracy
639 was not available.

640 iii. Bias in the leaf optical measurements

641 As highlighted in the introduction, the uncertainty associated to leaf optical measurements in the
642 NIR domain may be increased because of the incomplete collection of the light leaving the highly
643 scattering tissue (Merzlyak et al., 2002). Merzlyak et al. (2004) proposed a correcting factor for
644 transmittance based on the hypothesis that leaf absorption in the NIR domain from 780 to 900 nm is
645 negligible for healthy leaves. However this correcting factor is not adopted as a standard correction
646 by the community. In order to detect possible uncertainty in the optical measurements in the NIR
647 domain with our data, we tested our ML approach with *TS1* (training with a unique dataset) and
648 spectral information either from 1700 to 2400 nm or from 1400 to 2400 nm (results not showed).

649 For both *LMA* and *EWT*, the regression models applied on independent datasets performed
650 similarly for the two spectral domains considered, but systematically performed better than the
651 regression models trained with the spectral information from 900 to 2400 nm. However, they were
652 still outperformed by PROSPECT inversion. Such a result thus tends to confirm that leaf optical
653 measurements in the NIR domain might be affected by some experimental uncertainty.

654 The poor performances reported for the estimation of *LMA* with PROSPECT inversion using *IO1* are
655 therefore mainly explained by the use of the NIR domain, which is subject to inaccuracies, from a
656 modeling and/or from an experimental point of view. Based on our study, we cannot conclude on
657 the relative importance of one or the other factor. These two possibilities should then be considered

658 and tested using the methods proposed in the literature (Merzlyak et al., 2004; Qiu et al., 2018).
659 Finally, the difference between directional hemispherical measurements and bidirectional
660 measurements should be systematically accounted for and appropriate physical models should be
661 used with the type of data they are expected to simulate.

662

663 c. Influence of the sampling of the training dataset on machine learning algorithms

664 Our results highlight the strong influence of the training dataset on the performances of ML
665 methods, which is not an original result *per se*. However, the different training strategies tested here
666 show that regression models should be used with extreme care when they are applied on data which
667 were not collected in the exact same conditions as training data. Finally, the optimal training
668 strategy in our case, *TS3*, requires that each campaign aiming at collecting leaf optical properties in
669 order to estimate constituent content based on statistical/ML methods should include destructive
670 measurements to be used during the training step. This means that publicly available datasets such
671 as ANGERS and LOPEX should not be used as the only training datasets for the estimation of leaf
672 chemistry based on spectroscopy from independent datasets. The origin of the suboptimal
673 performances obtained in particular with *TS2* and *TS3* should also be investigated. ML algorithms are
674 currently mainly used for their predictive capacity. However, they can also as part of a descriptive
675 framework. Feilhauer et al. (2015) proposed an interesting illustration as they suggested combining
676 multiple methods in order to identify the most relevant spectral bands related to leaf chemistry,
677 based on both experimental and simulated data. Following the same method, the identification of
678 the spectral bands maximizing the generalization ability of ML algorithms by discarding spectral
679 domains prompt to experimental uncertainty or model approximations could be considered. Finally,
680 hybrid methods using simulated data during the training stage of a ML algorithm appear as an
681 interesting alternative to data-driven methods purely based on experimental data, and further

682 investigation is needed in order to define the proper strategy to generate such training dataset and
683 combine the generalization ability of physically-based approaches with the computational efficiency
684 of data-driven approaches.

685

686 d. Relevance of these results for leaf trait monitoring

687 The results obtained in this study contribute to a better understanding of the optimal remotely-
688 sensed monitoring of *LMA* and *EWT*, two key vegetation traits that convey multiple information
689 about the spatial and temporal variation in ecological and functional diversity of terrestrial
690 ecosystems. This can possibly contribute to facilitating the study of plant functions and their
691 interactions with and responses to the environment. As an example, Feilhauer et al. (2018) provide a
692 good illustration of the interest of remotely-sensed *LMA* for ecological analysis of wetland
693 vegetation, in particular for the better understanding of the effect of long-term drought on
694 ecosystem functions. They focused on *LMA* because of its plasticity in response to variable
695 environmental conditions, and its relationship with potential growth rate.

696 The estimation of these traits at the leaf scale now needs to be further investigated at the canopy
697 scale. In order to test the applicability of our approach at the canopy scale, the first step will consist
698 in working with a simulated dataset obtained with canopy reflectance models such as SAIL
699 (Jacquemoud et al., 2009; Verhoef, 1984) and DART (Gastellu-Etchegorry et al., 1996, 2015). The
700 direct application of model inversion based on iterative optimization restricts the complexity of the
701 canopy model, hence the type of vegetation to be investigated: the adaptation of our method
702 should be relatively straightforward when using PROSAIL on homogeneous canopy covers, but
703 hybrid methods should be considered when using DART simulations and working on heterogeneous
704 canopy covers.

705 An important challenge for the applicability of our results at the canopy scale is the low intensity of
706 the solar radiation in the optimal SWIR domain identified in this study, which usually leads to low
707 signal to noise ratio. Currently, hyperspectral information is mainly available from airborne imaging
708 spectroscopy (Asner et al., 2012; Schaepman et al., 2015). Asner et al. (2015) obtained accurate
709 estimation of *LMA* based on multivariate statistical methods applied on imaging spectroscopy for
710 heterogeneous canopies in tropical ecosystems, and they also concluded on the importance of the
711 spectral domain from 2000 nm to 2500 nm for a proper calibration of the regression models.
712 Recently, Feilhauer et al. (2018) reported good suitability of airborne imaging spectroscopy analyzed
713 with a hybrid method (Random forest trained with PROSAIL simulations) for *LMA* mapping in natural
714 ecosystems. Hyperion is the only spaceborne sensor, but the signal to noise ratio is known to be
715 relatively low (le Maire et al., 2008). The contribution of modeling through sensitivity studies
716 performed at canopy scale may therefore provide insightful information for the instrumental
717 specifications of future satellites dedicated to the monitoring of vegetation and environment such as
718 EnMAP, and for the development of algorithms (Jetz et al., 2016; Lee et al., 2015; Leitão et al., 2015).

719

720 6. CONCLUSIONS

721 In this paper, we compared the performances of various methods for the estimation of *EWT* and
722 *LMA* based on leaf reflectance and transmittance in the spectral domain ranging from 900 to 2400
723 nm. These methods included PROSPECT inversion based on iterative optimization with various merit
724 functions and machine learning (ML) algorithms with different training strategies. Six independent
725 datasets acquired from various vegetation types, including temperate, boreal and tropical
726 ecosystems were used in order to validate our results.

727 Our results showed that the poor performances of PROSPECT inversion reported in many studies for
728 the estimation of *LMA* could be dramatically improved when excluding spectral information in the

729 NIR domain from 900 to 1300 nm. We investigated the performances of PROSPECT inversion for the
730 estimation of *EWT* and *LMA* using multiple spectral subdomains, and identified an optimal spectral
731 domain ranging from 1700 to 2400 nm. Overall, PROSPECT inversion performed on this spectral
732 domain provided more accurate *LMA* and *EWT* estimates than ML algorithms trained on
733 experimental datasets. Unlike ML algorithms, PROSPECT inversion showed strong generalization
734 ability. Despite numerous studies showing the poor performances of PROSPECT for the estimation of
735 *LMA*, our study shows that model inversion using iterative optimization can outperform other
736 methods with an appropriate merit function, with no need for recalibration or training stage. By this
737 study, we therefore confirm the strong potential and accuracy of PROSPECT on critical spectral
738 domains. We also identified weaknesses which can be attributed either to physical modeling and
739 experimental acquisition of leaf optical properties in the NIR domain.

740 These results motivate further investigation involving hybrid methods for the estimation of *LMA* and
741 *EWT*, in order to take advantage of the computational efficiency of data-driven algorithms and
742 overcome limitations inherent to suboptimal experimental sampling of training data. Implications of
743 these results for the optimal estimation of *LMA* and *EWT* at the canopy scale will also be
744 investigated, as *LMA* and *EWT* are both key traits when monitoring ecosystem functions.

745

746 7. ACKNOWLEDGMENTS

747 The authors warmly thank Luc Bidel, Christophe François and Gabriel Pavan who collected the
748 ANGERS dataset. This work was funded by the TOSCA program grant of the French Space Agency
749 (CNES) (HyperTropik project); the International Network for Terrestrial Research and Monitoring in
750 the Arctic (INTERACT) (FLUO-SYNTHESIS project); the Brazilian Coordination for the Improvement of
751 Higher Education Personnel (CAPES). ITATINGA genotype test is funded in part by the EUCFLUX
752 project of Forestry Science and Research Institute (IPEF) and in part by SOERE F-ORE-T, which is

753 supported annually by Ecofor, Allenvi, and the ANAEE-F. The authors also thank Valentine Alt,
754 Samuel Council, and Philippe Gaucher for tree climbing and data collection, as well as Anna
755 Grandchamp for her help during data collection in Nouragues field station.

756

757 8. REFERENCES

- 758 Ali, A.M., Darvishzadeh, R., Skidmore, A.K., Duren, I. van, Heiden, U., Heurich, M., 2016. Estimating
759 leaf functional traits by inversion of PROSPECT: Assessing leaf dry matter content and
760 specific leaf area in mixed mountainous forest. *Int. J. Appl. Earth Obs. Geoinformation* 45,
761 66–76. <https://doi.org/10.1016/j.jag.2015.11.004>
- 762 Allen, W.A., Gausman, H.W., Richardson, A.J., 1970. Mean effective optical constants of cotton
763 leaves. *J. Opt. Soc. Am.* 60, 542–547. <https://doi.org/10.1364/JOSA.60.000542>
- 764 Allen, W.A., Gausman, H.W., Richardson, A.J., Thomas, J.R., 1969. Interaction of isotropic light with a
765 compact plant leaf. *J. Opt. Soc. Am.* 59, 1376–1379.
766 <https://doi.org/10.1364/JOSA.59.001376>
- 767 Antúnez, I., Retamosa, E.C., Villar, R., 2001. Relative growth rate in phylogenetically related
768 deciduous and evergreen woody species. *Oecologia* 128, 172–180.
769 <https://doi.org/10.1007/s004420100645>
- 770 Asner, G.P., Knapp, D.E., Boardman, J., Green, R.O., Kennedy-Bowdoin, T., Eastwood, M., Martin,
771 R.E., Anderson, C., Field, C.B., 2012. Carnegie Airborne Observatory-2: Increasing science
772 data dimensionality via high-fidelity multi-sensor fusion. *Remote Sens. Environ.* 124, 454–
773 465. <https://doi.org/10.1016/j.rse.2012.06.012>
- 774 Asner, G.P., Martin, R.E., 2016. Spectranomics: Emerging science and conservation opportunities at
775 the interface of biodiversity and remote sensing. *Glob. Ecol. Conserv.* 8, 212–219.
776 <https://doi.org/10.1016/j.gecco.2016.09.010>
- 777 Asner, G.P., Martin, R.E., Anderson, C.B., Knapp, D.E., 2015. Quantifying forest canopy traits: Imaging
778 spectroscopy versus field survey. *Remote Sens. Environ.* 158, 15–27.
779 <https://doi.org/10.1016/j.rse.2014.11.011>
- 780 Asner, G.P., Martin, R.E., Ford, A.J., Metcalfe, D.J., Liddell, M.J., 2009. Leaf chemical and spectral
781 diversity in Australian tropical forests. *Ecol. Appl.* 19, 236–253. <https://doi.org/10.1890/08-0023.1>
- 782
- 783 Asner, G.P., Martin, R.E., Tupayachi, R., Emerson, R., Martinez, P., Sinca, F., Powell, G.V., Wright, S.J.,
784 Lugo, A.E., 2011. Taxonomy and remote sensing of leaf mass per area (LMA) in humid
785 tropical forests. *Ecol. Appl.* 21, 85–98.
- 786 Baret, F., Buis, S., 2008. Estimating Canopy Characteristics from Remote Sensing Observations:
787 Review of Methods and Associated Problems, in: Liang, S. (Ed.), *Advances in Land Remote*
788 *Sensing*. Springer Netherlands, Dordrecht, pp. 173–201.
- 789 Barry, K., Newnham, G., 2012. Quantification of chlorophyll and carotenoid pigments in eucalyptus
790 foliage with the radiative transfer model PROSPECT 5 is affected by anthocyanin and
791 epicuticular waxes., in: *Proc. Geospatial Science Research 2 Symposium, GSR 2012*,
792 Melbourne, Australia, December 10-12, 2012.

793 Bousquet, L., Lachérade, S., Jacquemoud, S., Moya, I., 2005. Leaf BRDF measurements and model for
794 specular and diffuse components differentiation. *Remote Sens. Environ.* 98, 201–211.
795 <https://doi.org/10.1016/j.rse.2005.07.005>

796 Bowyer, P., Danson, F.M., 2004. Sensitivity of spectral reflectance to variation in live fuel moisture
797 content at leaf and canopy level. *Remote Sens. Environ.* 92, 297–308.
798 <https://doi.org/10.1016/j.rse.2004.05.020>

799 Breiman, L., 2001. Random Forests. *Mach. Learn.* 45, 5–32.
800 <https://doi.org/10.1023/A:1010933404324>

801 Brown, M., Lewis, H.G., Gunn, S.R., 2000. Linear spectral mixture models and support vector
802 machines for remote sensing. *IEEE Trans. Geosci. Remote Sens.* 38, 2346–2360.
803 <https://doi.org/10.1109/36.868891>

804 Carter, G.A., Knapp, A.K., 2001. Leaf optical properties in higher plants: linking spectral
805 characteristics to stress and chlorophyll concentration. *Am. J. Bot.* 88, 677–684.

806 Ceccato, P., Flasse, S., Tarantola, S., Jacquemoud, S., Grégoire, J.-M., 2001. Detecting vegetation leaf
807 water content using reflectance in the optical domain. *Remote Sens. Environ.* 77, 22–33.
808 [https://doi.org/10.1016/S0034-4257\(01\)00191-2](https://doi.org/10.1016/S0034-4257(01)00191-2)

809 Chang, C.-C., Lin, C.-J., 2011. LIBSVM: A library for support vector machines. *ACM Trans. Intell. Syst.*
810 *Technol.* 2, 1–27. <https://doi.org/10.1145/1961189.1961199>

811 Chapin, F.S., 2003. Effects of Plant Traits on Ecosystem and Regional Processes: a Conceptual
812 Framework for Predicting the Consequences of Global Change. *Ann. Bot.* 91, 455–463.
813 <https://doi.org/10.1093/aob/mcg041>

814 Chuvieco, E., Riaño, D., Aguado, I., Cocero, D., 2002. Estimation of fuel moisture content from
815 multitemporal analysis of Landsat Thematic Mapper reflectance data: Applications in fire
816 danger assessment. *Int. J. Remote Sens.* 23, 2145–2162.
817 <https://doi.org/10.1080/01431160110069818>

818 Colombo, R., Meroni, M., Marchesi, A., Busetto, L., Rossini, M., Giardino, C., Panigada, C., 2008.
819 Estimation of leaf and canopy water content in poplar plantations by means of hyperspectral
820 indices and inverse modeling. *Remote Sens. Environ.* 112, 1820–1834.
821 <https://doi.org/10.1016/j.rse.2007.09.005>

822 Conejo, E., Frangi, J.-P., de Rosny, G., 2015. Neural network implementation for a reversal procedure
823 for water and dry matter estimation on plant leaves using selected LED wavelengths. *Appl.*
824 *Opt.* 54, 5453. <https://doi.org/10.1364/AO.54.005453>

825 Cornelissen, J.H.C., Grootemaat, S., Verheijen, L.M., Cornwell, W.K., van Bodegom, P.M., van der
826 Wal, R., Aerts, R., 2017. Are litter decomposition and fire linked through plant species traits?
827 *New Phytol.* 216, 653–669. <https://doi.org/10.1111/nph.14766>

828 Cornelissen, J.H.C., Lavorel, S., Garnier, E., Díaz, S., Buchmann, N., Gurvich, D.E., Reich, P.B., Steege,
829 H. ter, Morgan, H.D., Heijden, M.G.A. van der, Pausas, J.G., Poorter, H., 2003. A handbook of
830 protocols for standardised and easy measurement of plant functional traits worldwide. *Aust.*
831 *J. Bot.* 51, 335. <https://doi.org/10.1071/BT02124>

832 Cortes, C., Vapnik, V., 1995. Support-vector networks. *Mach. Learn.* 20, 273–297.
833 <https://doi.org/10.1007/BF00994018>

834 Datt, B., 1999. Remote Sensing of Water Content in Eucalyptus Leaves. *Aust. J. Bot.* 47, 909–923.

835 Dawson, T.P., Curran, P.J., Plummer, S.E., 1998. The biochemical decomposition of slash pine needles
836 from reflectance spectra using neural networks. *Int. J. Remote Sens.* 19, 1433–1438.
837 <https://doi.org/10.1080/014311698215540>

838 de la Riva, E.G., Olmo, M., Poorter, H., Ubera, J.L., Villar, R., 2016. Leaf Mass per Area (LMA) and Its
839 Relationship with Leaf Structure and Anatomy in 34 Mediterranean Woody Species along a

840 Water Availability Gradient. *PLOS ONE* 11, e0148788.
841 <https://doi.org/10.1371/journal.pone.0148788>

842 Diaz, S., Cabido, M., 2001. Vive la diff?rence: plant functional diversity matters to ecosystem
843 processes. *Trends Ecol. Evol.* 16, 646–655. [https://doi.org/10.1016/S0169-5347\(01\)02283-2](https://doi.org/10.1016/S0169-5347(01)02283-2)

844 Drucker, H., Burges, C.J.C., Kaufman, L., C, C.J., Kaufman, B.L., Smola, A., Vapnik, V., 1996. Support
845 Vector Regression Machines.

846 Eviner, V.T., Chapin III, F.S., 2003. Functional Matrix: A Conceptual Framework for Predicting
847 Multiple Plant Effects on Ecosystem Processes. *Annu. Rev. Ecol. Evol. Syst.* 34, 455–485.
848 <https://doi.org/10.1146/annurev.ecolsys.34.011802.132342>

849 Feilhauer, H., Asner, G.P., Martin, R.E., 2015. Multi-method ensemble selection of spectral bands
850 related to leaf biochemistry. *Remote Sens. Environ.* 164, 57–65.
851 <https://doi.org/10.1016/j.rse.2015.03.033>

852 Feilhauer, H., Schmid, T., Faude, U., Sánchez-Carrillo, S., Cirujano, S., 2018. Are remotely sensed
853 traits suitable for ecological analysis? A case study of long-term drought effects on leaf mass
854 per area of wetland vegetation. *Ecol. Indic.* 88, 232–240.
855 <https://doi.org/10.1016/j.ecolind.2018.01.012>

856 Féret, J.-B., François, C., Asner, G.P., Gitelson, A.A., Martin, R.E., Bidet, L.P.R., Ustin, S.L., le Maire, G.,
857 Jacquemoud, S., 2008. PROSPECT-4 and 5: Advances in the leaf optical properties model
858 separating photosynthetic pigments. *Remote Sens. Environ.* 112, 3030–3043.
859 <https://doi.org/10.1016/j.rse.2008.02.012>

860 Féret, J.-B., François, C., Gitelson, A., Asner, G.P., Barry, K.M., Panigada, C., Richardson, A.D.,
861 Jacquemoud, S., 2011. Optimizing spectral indices and chemometric analysis of leaf chemical
862 properties using radiative transfer modeling. *Remote Sens. Environ.* 115, 2742–2750.

863 Féret, J.-B., Gitelson, A.A., Noble, S.D., Jacquemoud, S., 2017. PROSPECT-D: Towards modeling leaf
864 optical properties through a complete lifecycle. *Remote Sens. Environ.* 193, 204–215.
865 <https://doi.org/10.1016/j.rse.2017.03.004>

866 Gastellu-Etchegorry, J., Demarez, V., Pinel, V., Zagolski, F., 1996. Modeling radiative transfer in
867 heterogeneous 3-D vegetation canopies. *Remote Sens. Environ.* 58, 131–156.
868 [https://doi.org/10.1016/0034-4257\(95\)00253-7](https://doi.org/10.1016/0034-4257(95)00253-7)

869 Gastellu-Etchegorry, J.-P., Yin, T., Lauret, N., Cajgfinger, T., Gregoire, T., Grau, E., Féret, J.-B., Lopes,
870 M., Guilleux, J., Dedieu, G., Malenovský, Z., Cook, B., Morton, D., Rubio, J., Durrieu, S.,
871 Cazanave, G., Martin, E., Ristorcelli, T., 2015. Discrete anisotropic radiative transfer (DART 5)
872 for modeling airborne and satellite spectroradiometer and LIDAR acquisitions of natural and
873 urban landscapes. *Remote Sens.* 7, 1667–1701. <https://doi.org/10.3390/rs70201667>

874 Gitelson, A.A., Keydan, G.P., Merzlyak, M.N., 2006. Three-band model for noninvasive estimation of
875 chlorophyll, carotenoids, and anthocyanin contents in higher plant leaves. *Geophys. Res.*
876 *Lett.* 33, L11402. <https://doi.org/10.1029/2006GL026457>

877 Gratani, L., Varone, L., 2006. Long-time variations in leaf mass and area of Mediterranean evergreen
878 broad-leaf and narrow-leaf maquis species. *Photosynthetica* 44, 161–168.
879 <https://doi.org/10.1007/s11099-006-0001-1>

880 Gualtieri, J.A., 2009. The Support Vector Machine (SVM) Algorithm for Supervised Classification of
881 Hyperspectral Remote Sensing Data, in: Camps-Valls, G., Bruzzone, L. (Eds.), *Kernel Methods*
882 *for Remote Sensing Data Analysis*. John Wiley & Sons, Ltd, Chichester, UK, pp. 49–83.

883 Hornik, K., Stinchcombe, M., White, H., 1989. Multilayer feedforward networks are universal
884 approximators. *Neural Netw.* 2, 359–366. [https://doi.org/10.1016/0893-6080\(89\)90020-8](https://doi.org/10.1016/0893-6080(89)90020-8)

885 Hosgood, B., Jacquemoud, S., Andreoli, G., Verdebout, J., Pedrini, A., Schmuck, G., 1994. Leaf Optical
886 Properties Experiment 93 (LOPEX93) (European Commission No. EUR 16095 EN). Joint
887 Research Centre, Institute for Remote Sensing Applications.

888 Jacquemoud, S., Baret, F., 1990. PROSPECT: A model of leaf optical properties spectra. *Remote Sens.*
889 *Environ.* 34, 75–91. [https://doi.org/10.1016/0034-4257\(90\)90100-Z](https://doi.org/10.1016/0034-4257(90)90100-Z)

890 Jacquemoud, S., Ustin, S.L., Verdebout, J., Schmuck, G., Andreoli, G., Hosgood, B., 1996. Estimating
891 leaf biochemistry using the PROSPECT leaf optical properties model. *Remote Sens. Environ.*
892 56, 194–202. [https://doi.org/10.1016/0034-4257\(95\)00238-3](https://doi.org/10.1016/0034-4257(95)00238-3)

893 Jacquemoud, S., Verhoef, W., Baret, F., Bacour, C., Zarco-Tejada, P.J., Asner, G.P., François, C., Ustin,
894 S.L., 2009. PROSPECT+ SAIL models: A review of use for vegetation characterization. *Remote*
895 *Sens. Environ.* 113, S56–S66. <https://doi.org/doi:10.1016/j.rse.2008.01.026>

896 Jay, S., Bendoula, R., Hadoux, X., Féret, J.-B., Gorretta, N., 2016. A physically-based model for
897 retrieving foliar biochemistry and leaf orientation using close-range imaging spectroscopy.
898 *Remote Sens. Environ.* 177, 220–236. <https://doi.org/10.1016/j.rse.2016.02.029>

899 Jetz, W., Cavender-Bares, J., Pavlick, R., Schimel, D., Davis, F.W., Asner, G.P., Guralnick, R., Kattge, J.,
900 Latimer, A.M., Moorcroft, P., Schaepman, M.E., Schildhauer, M.P., Schneider, F.D., Schrod, F.,
901 Stahl, U., Ustin, S.L., 2016. Monitoring plant functional diversity from space. *Nat. Plants* 2,
902 16024. <https://doi.org/10.1038/nplants.2016.24>

903 Lardeux, C., Frison, P.-L., Tison, C., Souyris, J.-C., Stoll, B., Fruneau, B., Rudant, J.-P., 2009. Support
904 Vector Machine for Multifrequency SAR Polarimetric Data Classification. *IEEE Trans. Geosci.*
905 *Remote Sens.* 47, 4143–4152. <https://doi.org/10.1109/TGRS.2009.2023908>

906 le Maire, G., François, C., Dufrêne, E., 2004. Towards universal broad leaf chlorophyll indices using
907 PROSPECT simulated database and hyperspectral reflectance measurements. *Remote Sens.*
908 *Environ.* 89, 1–28. <https://doi.org/10.1016/j.rse.2003.09.004>

909 le Maire, G., François, C., Soudani, K., Berveiller, D., Pontailier, J.-Y., Bréda, N., Genet, H., Davi, H.,
910 Dufrêne, E., 2008. Calibration and validation of hyperspectral indices for the estimation of
911 broadleaved forest leaf chlorophyll content, leaf mass per area, leaf area index and leaf
912 canopy biomass. *Remote Sens. Environ.* 112, 3846–3864.

913 le Maire, G., Marsden, C., Nouvellon, Y., Grinand, C., Hakamada, R., Stape, J.-L., Laclau, J.-P., 2011.
914 MODIS NDVI time-series allow the monitoring of Eucalyptus plantation biomass. *Remote*
915 *Sens. Environ.* 115, 2613–2625. <https://doi.org/10.1016/j.rse.2011.05.017>

916 Lee, C.M., Cable, M.L., Hook, S.J., Green, R.O., Ustin, S.L., Mandl, D.J., Middleton, E.M., 2015. An
917 introduction to the NASA Hyperspectral InfraRed Imager (HyspIRI) mission and preparatory
918 activities. *Remote Sens. Environ.* 167, 6–19. <https://doi.org/10.1016/j.rse.2015.06.012>

919 Leitão, P., Schwieder, M., Suess, S., Okujeni, A., Galvão, L., Linden, S., Hostert, P., 2015. Monitoring
920 Natural Ecosystem and Ecological Gradients: Perspectives with EnMAP. *Remote Sens.* 7,
921 13098–13119. <https://doi.org/10.3390/rs71013098>

922 Li, D., Cheng, T., Jia, M., Zhou, K., Lu, N., Yao, X., Tian, Y., Zhu, Y., Cao, W., 2018. PROCWT: Coupling
923 PROSPECT with continuous wavelet transform to improve the retrieval of foliar chemistry
924 from leaf bidirectional reflectance spectra. *Remote Sens. Environ.* 206, 1–14.
925 <https://doi.org/10.1016/j.rse.2017.12.013>

926 Li, P., Wang, Q., 2011. Retrieval of leaf biochemical parameters using PROSPECT inversion: A new
927 approach for alleviating ill-posed problems. *IEEE Trans. Geosci. Remote Sens.* 49, 2499–
928 2506. <https://doi.org/10.1109/TGRS.2011.2109390>

929 Lucarini, V., Saarinen, J.J., Peiponen, K.-E., Vartiainen, E.M. (Eds.), 2005. *Kramers-Kronig relations in*
930 *optical materials research*, Springer series in optical sciences. Springer, Berlin.

931 Main, R., Cho, M.A., Mathieu, R., O’Kennedy, M.M., Ramoelo, A., Koch, S., 2011. An investigation
932 into robust spectral indices for leaf chlorophyll estimation. *ISPRS J. Photogramm. Remote*
933 *Sens.* 66, 751–761. <https://doi.org/10.1016/j.isprsjprs.2011.08.001>

934 Malenovský, Z., Albrechtová, J., Lhotáková, Z., Zurita-Milla, R., Clevers, J.G.P.W., Schaepman, M.E.,
935 Cudlín, P., 2006. Applicability of the PROSPECT model for Norway spruce needles. *Int. J.*
936 *Remote Sens.* 27, 5315–5340. <https://doi.org/10.1080/01431160600762990>

937 Merzlyak, M.N., Chivkunova, O.B., Melø, T.B., Naqvi, K.R., 2002. Does a leaf absorb radiation in the
938 near infrared (780–900 nm) region? A new approach to quantifying optical reflection,
939 absorption and transmission of leaves. *Photosynth. Res.* 72, 263–270.
940 <https://doi.org/10.1023/A:1019823303951>

941 Merzlyak, M.N., Melø, T.B., Razi Naqvi, K., 2004. Estimation of leaf transmittance in the near infrared
942 region through reflectance measurements. *J. Photochem. Photobiol. B* 74, 145–150.
943 <https://doi.org/10.1016/j.jphotobiol.2004.03.003>

944 Mobasheri, M.R., Fatemi, S.B., 2013. Leaf Equivalent Water Thickness assessment using reflectance
945 at optimum wavelengths. *Theor. Exp. Plant Physiol.* 25, 196–202.
946 <https://doi.org/10.1590/S2197-00252013005000001>

947 Newnham, G.J., Burt, T., 2001. Validation of a leaf reflectance and transmittance model for three
948 agricultural crop species. *IEEE*, pp. 2976–2978. <https://doi.org/10.1109/IGARSS.2001.978227>

949 Oliveira, J. de C., Feret, J.-B., Ponzoni, F.J., Nouvellon, Y., Gastellu-Etchegorry, J.-P., Campoe, O.C.,
950 Stape, J.L., Rodriguez, L.C.E., le Maire, G., 2017. Simulating the Canopy Reflectance of
951 Different Eucalypt Genotypes With the DART 3-D Model. *IEEE J. Sel. Top. Appl. Earth Obs.*
952 *Remote Sens.* 1–9. <https://doi.org/10.1109/JSTARS.2017.2690000>

953 Oren, R., Schulze, E.-D., Matyssek, R., Zimmermann, R., 1986. Estimating photosynthetic rate and
954 annual carbon gain in conifers from specific leaf weight and leaf biomass. *Oecologia* 70, 187–
955 193. <https://doi.org/10.1007/BF00379238>

956 Osnas, J.L.D., Lichstein, J.W., Reich, P.B., Pacala, S.W., 2013. Global Leaf Trait Relationships: Mass,
957 Area, and the Leaf Economics Spectrum. *Science* 340, 741–744.
958 <https://doi.org/10.1126/science.1231574>

959 Pérez-Harguindeguy, N., Díaz, S., Garnier, E., Lavorel, S., Poorter, H., Jaureguiberry, P., Bret-Harte,
960 M.S., Cornwell, W.K., Craine, J.M., Gurvich, D.E., Urcelay, C., Veneklaas, E.J., Reich, P.B.,
961 Poorter, L., Wright, I.J., Ray, P., Enrico, L., Pausas, J.G., de Vos, A.C., Buchmann, N., Funes, G.,
962 Quétier, F., Hodgson, J.G., Thompson, K., Morgan, H.D., ter Steege, H., Sack, L., Blonder, B.,
963 Poschlod, P., Vaieretti, M.V., Conti, G., Staver, A.C., Aquino, S., Cornelissen, J.H.C., 2013. New
964 handbook for standardised measurement of plant functional traits worldwide. *Aust. J. Bot.*
965 61, 167. <https://doi.org/10.1071/BT12225>

966 Poorter, H., Niinemets, Ü., Poorter, L., Wright, I.J., Villar, R., 2009. Causes and consequences of
967 variation in leaf mass per area (LMA): a meta-analysis. *New Phytol.* 182, 565–588.
968 <https://doi.org/10.1111/j.1469-8137.2009.02830.x>

969 Puglielli, G., Crescente, M.F., Frattaroli, A.R., Gratani, L., 2015. Leaf Mass Per Area (LMA) as a
970 Possible Predictor of Adaptive Strategies in Two Species of *Sesleria* (Poaceae): Analysis of
971 Morphological, Anatomical and Physiological Leaf Traits. *Ann. Bot. Fenn.* 52, 135–143.
972 <https://doi.org/10.5735/085.052.0201>

973 Qiu, F., Chen, J.M., Ju, W., Wang, J., Zhang, Q., Fang, M., 2018. Improving the PROSPECT Model to
974 Consider Anisotropic Scattering of Leaf Internal Materials and Its Use for Retrieving Leaf
975 Biomass in Fresh Leaves. *IEEE Trans. Geosci. Remote Sens.* 56, 3119–3136.
976 <https://doi.org/10.1109/TGRS.2018.2791930>

- 977 Rees, M., Osborne, C.P., Woodward, F.I., Hulme, S.P., Turnbull, L.A., Taylor, S.H., 2010. Partitioning
978 the Components of Relative Growth Rate: How Important Is Plant Size Variation? *Am. Nat.*
979 176, E152–E161. <https://doi.org/10.1086/657037>
- 980 Reich, P.B., Walters, M.B., Ellsworth, D.S., 1997. From tropics to tundra: global convergence in plant
981 functioning. *Proc. Natl. Acad. Sci. U. S. A.* 94, 13730–13734.
- 982 Reich, P.B., Walters, M.B., Ellsworth, D.S., Vose, J.M., Volin, J.C., Gresham, C., Bowman, W.D., 1998.
983 Relationships of leaf dark respiration to leaf nitrogen, specific leaf area and leaf life-span: a
984 test across biomes and functional groups. *Oecologia* 114, 471–482.
985 <https://doi.org/10.1007/s004420050471>
- 986 Réjou-Méchain, M., Tymen, B., Blanc, L., Fauset, S., Feldpausch, T.R., Monteagudo, A., Phillips, O.L.,
987 Richard, H., Chave, J., 2015. Using repeated small-footprint LiDAR acquisitions to infer spatial
988 and temporal variations of a high-biomass Neotropical forest. *Remote Sens. Environ.* 169,
989 93–101. <https://doi.org/10.1016/j.rse.2015.08.001>
- 990 Riano, D., Vaughan, P., Chuvieco, E., Zarco-Tejada, P.J., Ustin, S.L., 2005. Estimation of fuel moisture
991 content by inversion of radiative transfer models to simulate equivalent water thickness and
992 dry matter content: analysis at leaf and canopy level. *IEEE Trans. Geosci. Remote Sens.* 43,
993 819–826. <https://doi.org/10.1109/TGRS.2005.843316>
- 994 Romero, A., Aguado, I., Yebra, M., 2012. Estimation of dry matter content in leaves using normalized
995 indexes and PROSPECT model inversion. *Int. J. Remote Sens.* 33, 396–414.
996 <https://doi.org/10.1080/01431161.2010.532819>
- 997 Schaeppman, M.E., Jehle, M., Hueni, A., D’Odorico, P., Damm, A., Weyermann, J., Schneider, F.D.,
998 Laurent, V., Popp, C., Seidel, F.C., Lenhard, K., Gege, P., Kuchler, C., Brazile, J., Kohler, P., De
999 Vos, L., Meuleman, K., Meynart, R., Schläpfer, D., Kneubühler, M., Itten, K.I., 2015. Advanced
1000 radiometry measurements and Earth science applications with the Airborne Prism
1001 Experiment (APEX). *Remote Sens. Environ.* 158, 207–219.
1002 <https://doi.org/10.1016/j.rse.2014.11.014>
- 1003 Schaeppman-Strub, G., Schaeppman, M.E., Painter, T.H., Dangel, S., Martonchik, J.V., 2006. Reflectance
1004 quantities in optical remote sensing—definitions and case studies. *Remote Sens. Environ.*
1005 103, 27–42. <https://doi.org/10.1016/j.rse.2006.03.002>
- 1006 Schimel, D., Pavlick, R., Fisher, J.B., Asner, G.P., Saatchi, S., Townsend, P., Miller, C., Frankenberg, C.,
1007 Hibbard, K., Cox, P., 2015. Observing terrestrial ecosystems and the carbon cycle from space.
1008 *Glob. Change Biol.* 21, 1762–1776. <https://doi.org/10.1111/gcb.12822>
- 1009 Schmitter, P., Steinrücken, J., Römer, C., Ballvora, A., Léon, J., Rascher, U., Plümer, L., 2017.
1010 Unsupervised domain adaptation for early detection of drought stress in hyperspectral
1011 images. *ISPRS J. Photogramm. Remote Sens.* 131, 65–76.
1012 <https://doi.org/10.1016/j.isprsjprs.2017.07.003>
- 1013 Stumpf, A., Kerle, N., 2011. Object-oriented mapping of landslides using Random Forests. *Remote*
1014 *Sens. Environ.* 115, 2564–2577. <https://doi.org/10.1016/j.rse.2011.05.013>
- 1015 Sun, J., Shi, S., Yang, J., Du, L., Gong, W., Chen, B., Song, S., 2018. Analyzing the performance of
1016 PROSPECT model inversion based on different spectral information for leaf biochemical
1017 properties retrieval. *ISPRS J. Photogramm. Remote Sens.* 135, 74–83.
1018 <https://doi.org/10.1016/j.isprsjprs.2017.11.010>
- 1019 Verhoef, W., 1984. Light scattering by leaf layers with application to canopy reflectance modeling:
1020 The SAIL model. *Remote Sens. Environ.* 16, 125–141. [https://doi.org/10.1016/0034-](https://doi.org/10.1016/0034-4257(84)90057-9)
1021 [4257\(84\)90057-9](https://doi.org/10.1016/0034-4257(84)90057-9)
- 1022 Verrelst, J., Camps-Valls, G., Muñoz-Marí, J., Rivera, J.P., Veroustraete, F., Clevers, J.G.P.W., Moreno,
1023 J., 2015. Optical remote sensing and the retrieval of terrestrial vegetation bio-geophysical

1024 properties – A review. *ISPRS J. Photogramm. Remote Sens.* 108, 273–290.
 1025 <https://doi.org/10.1016/j.isprsjprs.2015.05.005>
 1026 Verrelst, J., Rivera, J.P., Gitelson, A., Delegido, J., Moreno, J., Camps-Valls, G., 2016. Spectral band
 1027 selection for vegetation properties retrieval using Gaussian processes regression. *Int. J. Appl.*
 1028 *Earth Obs. Geoinformation* 52, 554–567. <https://doi.org/10.1016/j.jag.2016.07.016>
 1029 Violle, C., Navas, M.-L., Vile, D., Kazakou, E., Fortunel, C., Hummel, I., Garnier, E., 2007. Let the
 1030 concept of trait be functional! *Oikos* 116, 882–892. [https://doi.org/10.1111/j.2007.0030-](https://doi.org/10.1111/j.2007.0030-1299.15559.x)
 1031 [1299.15559.x](https://doi.org/10.1111/j.2007.0030-1299.15559.x)
 1032 Wang, L., Qu, J.J., Hao, X., Hunt, E.R., 2011. Estimating dry matter content from spectral reflectance
 1033 for green leaves of different species. *Int. J. Remote Sens.* 32, 7097–7109.
 1034 <https://doi.org/10.1080/01431161.2010.494641>
 1035 Wang, Z., Skidmore, A.K., Wang, T., Darvishzadeh, R., Hearne, J., 2015. Applicability of the PROSPECT
 1036 model for estimating protein and cellulose+lignin in fresh leaves. *Remote Sens. Environ.* 168,
 1037 205–218. <https://doi.org/10.1016/j.rse.2015.07.007>
 1038 Weng, E., Fariori, C.E., Dybzinski, R., Pacala, S.W., 2017. Predicting vegetation type through
 1039 physiological and environmental interactions with leaf traits: evergreen and deciduous
 1040 forests in an earth system modeling framework. *Glob. Change Biol.* 23, 2482–2498.
 1041 <https://doi.org/10.1111/gcb.13542>
 1042 Wright, I.J., Reich, P.B., Westoby, M., Ackerly, D.D., Baruch, Z., Bongers, F., Cavender-Bares, J.,
 1043 Chapin, T., Cornelissen, J.H.C., Diemer, M., Flexas, J., Garnier, E., Groom, P.K., Gulias, J.,
 1044 Hikosaka, K., Lamont, B.B., Lee, T., Lee, W., Lusk, C., Midgley, J.J., Navas, M.-L., Niinemets, Ü.,
 1045 Oleksyn, J., Osada, N., Poorter, H., Poot, P., Prior, L., Pyankov, V.I., Roumet, C., Thomas, S.C.,
 1046 Tjoelker, M.G., Veneklaas, E.J., Villar, R., 2004. The worldwide leaf economics spectrum.
 1047 *Nature* 428, 821–827. <https://doi.org/10.1038/nature02403>
 1048 Yebra, M., Dennison, P.E., Chuvieco, E., Riaño, D., Zylstra, P., Hunt, E.R., Danson, F.M., Qi, Y., Jurdao,
 1049 S., 2013. A global review of remote sensing of live fuel moisture content for fire danger
 1050 assessment: Moving towards operational products. *Remote Sens. Environ.* 136, 455–468.
 1051 Zhang, X.M., He, G.J., Zhang, Z.M., Peng, Y., Long, T.F., 2017. Spectral-spatial multi-feature
 1052 classification of remote sensing big data based on a random forest classifier for land cover
 1053 mapping. *Clust. Comput.* 20, 2311–2321. <https://doi.org/10.1007/s10586-017-0950-0>
 1054
 1055

1056 9. LIST OF FIGURE CAPTIONS

1057 **Figure 1.** Normalized *RMSE* (*NRMSE*, in %) obtained for *EWT* with PROSPECT inversion method *IO3*
1058 over each dataset and each reduced spectral domains bounded by a starting wavelength λ_1 (y-axis)
1059 and an ending wavelength λ_2 (x-axis). The normalization is specific to each dataset based on the
1060 performances of *IO1* (*NRMSE*=100%, lower right corner). The green star indicates the spectral
1061 segment producing the best results.

1062 **Figure 2.** Normalized *RMSE* (*NRMSE*, in %) obtained for *LMA* estimation with PROSPECT inversion
1063 method *IO3*, over each dataset and each reduced spectral domains bounded by a starting
1064 wavelength λ_1 (y-axis) and an ending wavelength λ_2 (x-axis). The normalization is specific to each
1065 dataset based on the performances of *IO1* (*NRMSE*=100%, lower right corner). The green star
1066 indicates the spectral segment producing the best results.

1067 **Figure 3.** Mean normalized *RMSE* values (*NRMSE*, in %) obtained for the estimation of *EWT* (left),
1068 *LMA* (center), and both constituents (right), after PROSPECT inversion over all experimental datasets
1069 pooled and each of the 120 spectral domains defined in Section 3.b. The green star indicates the
1070 spectral segment producing the best results.

1071 **Figure 4.** *EWT* estimation results obtained using PROSPECT inversion (*IO1*, *IO2*, *IO3*) and ML
1072 regression (training sampling *TS2*).

1073 **Figure 5.** *LMA* estimation results obtained using PROSPECT inversion (*IO1*, *IO2*, *IO3*) and SVM
1074 regression (training sampling *TS2*).

1075